UNIVERSITY OF CALIFORNIA

Radiation Laboratory

BERKELEY, CALIFORNIA

UCRL-1408
Unclassified - Physics Distribution

UNIVERSITY OF CALIFORNIA

Radiation Laboratory

Contract No. W-7405-eng-48

ELASTIC SCATTERING OF 340 MEV PROTONS

Robert E. Richardson

(Thesis)

July 26, 1951

Berkeley, California

TABLE OF CONTENTS

LIST OF FIGURES

I INTRODUCTION AND PURPOSE

A. Previous Diffraction Experiments

Elastic scattering of high energy nucleons by nuclei is analogous to optical Fraunhofer diffraction considering the nucleus as the scattering obstacle and using the DeBroglie wavelength ($\lambda = h/p$) of the high energy nucleons as the incident wavelength.

Amaldi, et al.[1] have observed the angular distribution of 14 Mev neutrons scattered from Pb nuclei, using neutrons produced by the D + Li reaction. The neutrons had a DeBroglie wavelength of 7.5×10^{-13} cm and were nearly monoenergetic, making them useful for seeking diffraction effects in heavy nuclei. The angular distribution observed had a strong forward peak, with a minimum at about 25° and a small secondary maximum near 40°. Assuming that the Pb nucleus behaved as an opaque sphere, they deduced from the position of the minimum that the radius of the Pb nucleus was about 1×10^{-12} cm.

Using the 90 Mev neutron beam of the 184-inch synchrocyclotron, Bratenahl, Fernbach, Hildebrand, Leith, and Moyer[2] have investigated the diffraction of neutrons by Be, C, Al, Cu, Ag, and Pb. The minima in their patterns were obscured by the energy spread of the neutron beam, which is produced by stripping of 190 Mev deuterons in a one-half inch thick Be target placed in the circulating dueteron beam.[3]

---

[1] E. Amaldi, D. Bocciarelli, B. N. Cacciapuoti, and G. C. Trabacchi, Nuovo Cimiento 3, 15-21, 203 (1946)

[2] A. Bratenahl, S. Fernbach, R. H. Hildebrand, C. E. Leith, and B. J. Moyer, Phys. Rev. 77, 597-605 (1950)

[3] R. Serber, Phys. Rev. 72, 1008 (1947)

The differential scattering cross sections were observed to be not zero in the region of expected secondary maxima for the heavier elements. Their results at the center of the forward peaks were well-described by the opaque nucleus picture, but at larger angles the predictions of the transparent nucleus theory of Fernbach, Serber, and Taylor[4] gave a better fit to the experimental points.[5]

Transparency of a spherical nucleus should alter the shape of the diffraction pattern by increasing the intensity in the region of the minima, decreasing the intensities of the secondary maxima, and causing the entire pattern to broaden slightly corresponding to a slight decrease in radius.

The present experiment makes use of higher energy and better energy resolution in an attempt to choose between the various nuclear models, and to determine nuclear radii as a check of previous works. The differential cross sections may be integrated and compared with the total cross sections of Bratenahl, et al., of Cook, McMillan, Peterson, and Sewell[6] at 90 Mev, of DeJuren and Knable[7] at 95 Mev, and of DeJuren and Moyer[8] at energies from 95 Mev to 270 Mev. These

---

[4] S. Fernbach, R. Serber, and T. B. Taylor, Phys. Rev. 75, 1352 (1949)

[5] It has recently been pointed out by Pasternack and Snyder, Phys. Rev. 80, 921 (1951), that the calculational method may introduce some error into the theoretical curves. By using an integration method instead of evaluating a series of Legendre polynomials, they were able to match the transparent nucleus model to the experimental points at very small angles as well as at wider angles.

[6] L. J. Cook, E. M. McMillan, J. M. Peterson, and D. C. Sewell, Phys. Rev. 75, 7 (1949)

[7] James DeJuren and Norman Knable, Phys. Rev. 77, 606 (1950)

[8] J. DeJuren and B. J. Moyer, Phys. Rev. 81, 919 (1951)

are all neutron experiments, but the results may be related to the proton results. Because of the Rutherford scattering, the curve to be integrated must be corrected at small angles in order to compare with neutron results (see Section V, B).

B. Wavelength of Particles in Present Experiment

Bratenahl, et al. consider the energy distribution of their neutron beam and the energy dependence of their detection efficiency to arrive at an effective energy of 83 Mev for their particles, giving a DeBroglie wavelength of 3.05×10^{-13} cm. The wavelength of the 340 Mev protons used in the present experiment is 1.43×10^{-13} cm. This shorter wavelength causes the diffraction patterns to be more concentrated in the forward direction, making intensities higher and thus more easily observable above background. This narrowing also makes necessary the use of instruments of high angular resolution in order to detect the details of the diffraction pattern.

C. Relative Merits of Neutrons and Protons

Protons have several advantages over neutrons in nuclear diffraction experiments. It is very easy to select monoenergetic protons by means of magnetic fields and slits. The use of monoenergetic particles greatly simplifies the interpretation of the results, since it prevents "washing out" of the minima due to energy spread.

The efficiency of charged-particle detectors is much higher than the efficiency of high-energy neutron detectors. The detection threshold for proton counters may be easily fixed by insertion of energy-attenuating material of the proper thickness, thus insuring that

essentially all of the particles counted are elastically scattered and that there is very little contamination from inelastically scattered particles.

There are some disadvantages to protons, however. The "pure" nuclear scattering is distorted by Rutherford scattering of the proton by the nuclear charge. The nuclear and Rutherford scattering are coherent, so there may be interference between them, but the energy of this experiment is high enough that Rutherford scattering is important only at very small angles, and is negligible in the region of the minima and secondary maxima.

Protons are multiply scattered in air and in the scattering target. This must be considered in determining the angular resolution. The energy loss due to ionization must be considered in determining the energy threshold.

D. Electric Quadrupole Moment

If the shape of the nucleus is ellipsoidal rather than spherical, and the nuclei are randomly oriented in the scattering target, the diffraction pattern may be expected to be altered in much the same way as the alteration due to nuclear transparency. Since the nuclear electric quadrupole moment is considered to be a measure of the departure from spherical symmetry, the results of this experiment may be used to set upper limits upon the electric quadrupole moments of the nuclei measured. In order to separate the transparency effects from the quadrupole moment effects the diffraction pattern of a nucleus known to have a high spin is compared with those of its neighbors having spins of zero or one-half. Nuclei of spin zero or one-half are expected to have

spherical symmetry since their spins are not able to establish a preferred axis. The transparency effect is expected to be a smooth function of atomic mass number.

II THEORY

A. Coulomb Correction

The exact solution of the wave equation involving both Coulomb and nuclear force fields is in a series of confluent hypergeometric functions. Since the bombarding energy in this experiment is much higher than the Coulomb barrier energies of the nuclei involved, the effects of the Coulomb field will be neglected as a first approximation. Therefore the theory will be given for the neutron case, with corrections which should come out of the exact solution indicated.

B. Neutron Solution in Partial Waves[9]

The wave function for the scattered neutron wave, which is obtained by subtracting the expression for the unperturbed incident plane wave from the solution for the case in which the scattering nucleus is present, may be represented asymptotically at large distance r from the scattering center, and at an angle θ from the direction of the incident beam by

$$\Psi_{\text{scatt}} \simeq \frac{e^{ikr}}{2ikr} \sum_{\ell=0}^{\infty} (2\ell + 1)(e^{2i\delta_\ell} - 1) P_\ell (\cos \theta), \qquad (1)$$

---

[9] The method of solution in partial waves was originated by J. W. Strutt (Lord Rayleigh), and presented in Proc. Lond. Math. Soc. (1) IV, 253 (1873), as a method of solution for optical problems. Its application to nuclear physics is presented in most standard texts on wave mechanics. (See for example, Leonard I. Schiff, Quantum Mechanics, McGraw Hill Book Company, Inc. (1949), pp. 103-121.)

where δ_ℓ is determined by matching the solution of the wave equation in the field-free region to that within the boundaries of the scattering potential. If there is no absorption in the scattering nucleus, δ_ℓ is a real number measuring the phase shift between the ℓth partial wave in the diverging components of the wave function with scatterer present and the corresponding ℓth component of the unperturbed plane wave. In the case in which absorption is also present, δ_ℓ is a complex number,

$$\delta_\ell = d_\ell + i\beta\ell \tag{2}$$

where β_ℓ is the exponent determining the absorption of the ℓth partial wave.

The ℓth partial wave may be identified with particles in the beam which have an angular momentum equal to $\ell\hbar$ with respect to the center of mass of the system, which is practically the center of mass of the scattering nucleus. Since the wavelength of the incident particles is appreciably smaller than the nuclear radius, it makes sense to speak of the particle colliding within the area represented by the cross section of the nucleus. If the impact parameter is b, the angular momentum, which is equal to the product of the linear momentum and the impact parameter, is allowed the values

$$pb = \ell\hbar, \text{ from which } \ell = \frac{pb}{\hbar} = \frac{b}{\lambda\!\!\!^{-}} = kb \tag{3}$$

For the Pb nucleus, values of ℓ up to nearly $\ell = 40$ should be allowed, for 340 Mev particles, since the largest value of impact parameter at which nuclear forces can be felt is equal to R, the nuclear radius. Particles passing at larger distances should be

unaffected, so that no components of the scattered beam should arise from $\ell > kR$.

The corresponding solution for the proton case would contain, besides δ_ℓ, an additional phase shift[10]

$$\epsilon_\ell = \eta_\ell - n \ln 2kr, \tag{4}$$

where n depends upon the charges, masses, and relative velocities of the interacting proton and nucleus, and η_ℓ is the argument of a Γ function which depends upon n and ℓ. Thus the method of partial waves is not strictly applicable to the proton case, but gives an asymptotic solution independent of r only for force fields of finite range. The higher values of ℓ which would be introduced by the Coulomb field give contributions to the cross section only at extremely small angles.

C. Nuclear Transparency

In the opaque nucleus theory it is considered that all particles which strike the nucleus are "absorbed," i.e., removed from the high energy beam by inelastic processes. In this case β_ℓ will be infinite for $0 \leq \ell \leq kR$, and zero for ℓ greater than kR. Thus for the perfectly absorbing sphere the scattered wave, Equation (1), becomes

$$\Psi_{\text{scatt}} \simeq - \frac{e^{ikr}}{2ikr} \sum_{\ell=0}^{\ell<kR} (2\ell + 1) P_\ell (\cos\theta) \tag{5}$$

It is interesting to note that these components of the scattered wave are just the corresponding outgoing components of the unperturbed plane wave shifted in phase by 180°. This is equivalent to removing these

---

[10] Schiff, op. cit., page 119

outgoing components from the total wave field, which is just what would be expected from a perfectly absorbing sphere and is an example of Babinet's principle from physical optics.

The differential scattering cross section per unit solid angle which is just the square of the amplitude of the scattered wave multiplied by r^2, is seen to be

$$\frac{d\sigma}{d\Omega}(\theta) = \frac{1}{4k^2}\left[\sum_{\ell=0}^{\ell<kR}(2\ell+1)\,P_\ell(\cos\theta)\right]^2 \qquad (6)$$

This distribution is equivalent to the optical Fraunhofer diffraction pattern of plane light waves of wavelength $\lambda = 2\pi/k$ by an opaque disk of radius $R' = R + 1/k$. It is usually given for small angles as

$$\frac{d\sigma}{d\Omega}(\theta) = \frac{1}{4}k^2 (R')^4 \left[\frac{J_1(2kR' \sin\frac{1}{2}\theta)}{kR' \sin\frac{1}{2}\theta}\right]^2 \qquad (7)$$

where J_1 is a first-order Bessel function.

If there is not complete absorption of those particles which strike the nucleus, the problem is one of diffraction of the incident wave by a sphere of material characterized by an index of refraction and an absorption coefficient. The index of refraction is due to the fact that the magnitude of the propagation vector may change within the nucleus due to the nuclear potential well. The absorption coefficient arises from interaction of the incident particle with individual nucleons in the nucleus, which is postulated to be the method of removing particles from the beam by giving rise to inelastic scattering. The absorption coefficient used by Fernbach, Serber, and Taylor is just the numerical density of nucleons in the nucleus multiplied by the nucleon-nucleon scattering cross sections

obtained from n-p and p-p scattering experiments and modified to allow for the suppression of small momentum transfers in the nucleus due to the Pauli exclusion principle. They obtain for a spherical scatterer with a nonreflecting surface:

$$\Psi_{\text{scatt}} \simeq \frac{e^{ikr}}{2ikr} \sum_{\ell=0}^{\ell+\frac{1}{2}<kR} (2\ell+1)\left[e^{(-K+2ik_1)s_\ell}-1\right] P_\ell(\cos\theta) \quad (8)$$

where k_1 is the change in propagation constant upon entering the nucleus, K is the absorption coefficient given by

$$K = \frac{3}{4\pi R^3}\left[Z\frac{2}{3}\sigma_{np(\text{free})} + (A-Z)\frac{1}{4}\left(\frac{2}{3}\sigma_{np(\text{free})}\right)\right] \quad (9)$$

and s_ℓ is essentially the path length, within the nucleus, of the particle having angular momentum equal to $\ell\hbar$,

$$s_\ell = \frac{\left[k^2R^2-(\ell+\frac{1}{2})^2\right]^{1/2}}{k} \quad (10)$$

The criterion for nonreflection is that the potential must not change appreciably within one wavelength. The factor of 2/3 comes from the suppression of small momentum transfers to nucleons within the nucleus due to the exclusion principle reducing the number of states available to the struck nucleon. The 1/4 comes from the action of the exclusion principle in excluding certain interaction states for p-p collisions.

III EXPERIMENTAL PROCEDURE

A. General Method

In Fig. 1 is shown a diagram of the experimental layout. The collimated external proton beam of the 184-inch synchrocyclotron beam is monitored by an argon-filled ionization chamber whose collected charge is integrated electronically. The scatterer, which is a thin sheet of material with a cross-sectional area considerably greater than the beam area, is placed in the beam, and the scattered protons are detected by a triple-coincidence scintillation counter proton telescope which is shielded from particles which may scatter from the mouth of the collimator or from the ionization chamber. The number of incident protons is determined by the charge collected by the ionization chamber, and the number of protons scattered at an angle θ into the solid angle offered by the telescope is determined by the number of counts from the telescope. These two numbers may be used to determine the differential scattering cross section, as is shown in Section V.

B. Source of the Protons

When a thin scatterer is placed in the full energy circulating proton beam of the 184-inch synchrocyclotron some of the protons are multiply scattered at such an angle that they enter the magnetic deflecting channel[11] and are removed from the main vacuum chamber into an evacuated tube which carries them through an opening in the main concrete shielding into a separate shielded enclosure usually referred to as the "cave," as shown in Fig. 1. The duration of the scattered beam

---

[11] C. E. Leith, Phys. Rev. 78, 89 (1950)

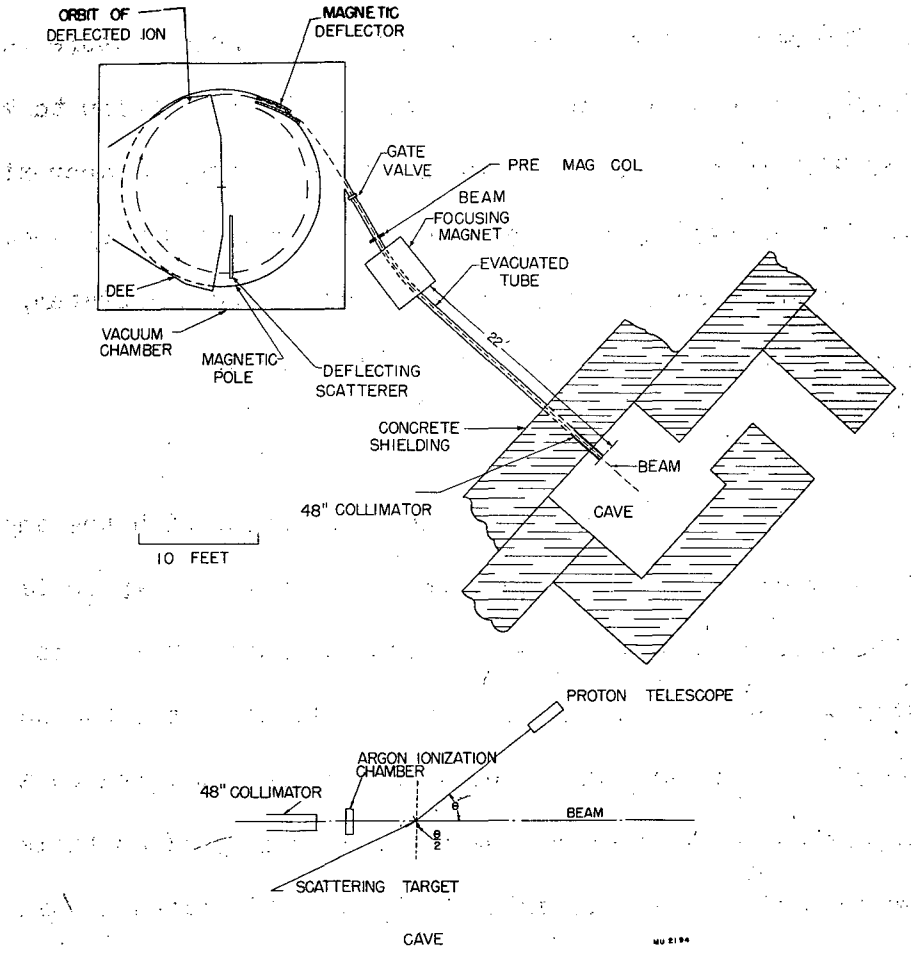
ORBIT OF DEFLECTED ION
MAGNETIC DEFLECTOR
GATE VALVE
PRE MAG COL
BEAM FOCUSING MAGNET
EVACUATED TUBE
DEE
VACUUM CHAMBER
MAGNETIC POLE
DEFLECTING SCATTERER
22°
CONCRETE SHIELDING
BEAM
48" COLLIMATOR
CAVE
10 FEET
PROTON TELESCOPE
ARGON IONIZATION CHAMBER
48" COLLIMATOR
BEAM
θ
θ/2
SCATTERING TARGET
CAVE

Fig. 1

pulse is 20-30 microseconds with a repetition rate of 50-60 per second. The energy of the protons which are accepted is determined by the path in the magnetic deflecting channel and by the path through the beam focusing magnet which directs them down the straight portion of the evacuated tube into the cave. The energy of this beam is known from the curvature in the magnetic field, and has also been measured as described below to have a range in Cu of 93.7 gm/cm^2 which corresponds to an energy of approximately 340 Mev. The energy may vary by a few Mev from one day to another due to slight differences in the setting up of the deflecting system, but the variation is certainly not more than $\pm$ 1 percent.

C. Collimation

The beam is collimated to the proper size consistent with the angular resolution desired by means of a 48-inch long brass plug which is inserted into the evacuated tube where it passes through the 15-foot concrete shielding. For most of the runs, the collimator used had an inside diameter of 1/2 inch and was tapered toward the outer end to a diameter of 3/4 inch in order to decrease the probability of multiple scattering from the collimator back into the beam. This gives a beam at the scatterer of approximately 5/8-inch diameter. In order to cut down the background of neutrons and gamma-rays due to the stopping of protons in the collimator, a collimating slit is placed in the beam just prior to the beam focusing magnet. Those protons which do not pass through the slit lose enough energy in the collimator wall so that they are over-deflected in the beam focusing magnet and do not find their way down the evacuated tube to the cave. For the high angular resolution runs, the circular collimator in the shielding was replaced by a

rectangular collimator in order that the scattered beam might appear to come from a line source instead of a cicrular source, thus increasing the angular resolution without at the same time introducing too much of a decrease in counting rate.

During the course of this experiment it was discovered that when the premagnet collimator is wide open the cross section of the beam as it enters the cave is concentrated mainly in a line about 1/32 inch thick, and tilted at an angle of about 13° to the horizontal, as shown in Fig. 2. The rectangular collimator used is 3/16 in. x 3/4 in. When it is used to replace a 1/2-inch diameter circular collimator, the counting rate is not appreciably changed. The rectangular collimator is tilted to line up with the beam cross section.

D. Setting of the Scatterer

In order that all of the protons elastically scattered into the telescope at any given angle will have traversed the same path length and thus have lost the same amount of energy by ionization in the target, the scatterer is not placed perpendicular to the beam, but is inclined to the perpendicular at half the angle by which the telescope is inclined to the beam.

E. Counting Rate, Background, Accidentals

The triple coincidence counting rate is kept to about one count per beam pulse by controlling the beam intensity. At this counting rate, the number of accidental triple coincidences is negligible, as determined by observing the counting rate as a function of beam intensity. The counting rates in the individual photomultipliers are much higher than this. They are, in fact, sometimes so high that the mechanical

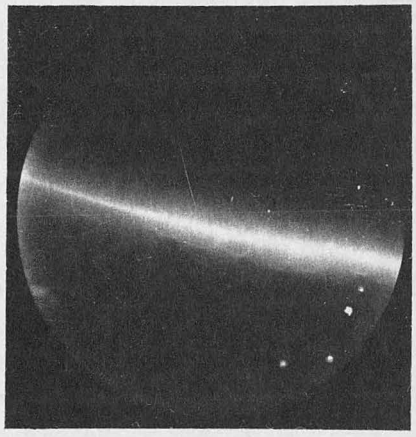

FIG. 2

registers of the scalers can not follow them. Since the coincidence unit has a high resolving time better than the scalers by nearly a factor of a hundred, this high individual counting rate is not objectionable, as is borne out by the determination of accidentals by varying the beam intensity.

After each datum run, a run is made under the same conditions except that the scattering target is removed to determine background. The background is considered in determining the magnitude of the effect as well as in determining the statistical accuracy of the points. The background is comparable to the true counting rate near and after the first minima of the diffraction pattern, necessitating the making of long datum runs and long background runs in order to obtain points of statistical significance in this region.

In order to eliminate any slowly varying instrumental errors such as voltage drift from apparently changing the shape of the diffraction pattern, the datum points are not taken for the angles in numerical order, but are taken at angles much farther apart than the spacing desired in the final points, with the intermediate points taken later. If the points taken later were not consistent with the initial points, suspicion would be directed toward such instrumental errors.

F. Detection Threshold and Absorption by the Energy Attenuators

In order to determine the detection efficiency of the proton telescope and to set the detection threshold, the telescope was placed in the direct beam with no scatterer present, and the counting rate measured as a function of the thickness of Cu energy attenuator present. For this run, the beam intensity was so low that the argon ionization chamber could not be used as a monitor. Therefore, the double coincidence counts of

the first two scintillators, which are before the energy attenuator, were used as a monitor. Because of the thickness of the scintillators and their holders, the curve could not be continued to zero thickness. The curve is shown in Fig. 3, and it is seen that the curve may be extrapolated to a ratio of unity from a thickness corresponding to the Cu equivalent of the scintillators and their duraluminum holders. The curve is seen to cut off at an equivalent thickness of 93.7 gm/cm^2 of Cu (mean range), which corresponds to 340 Mev on the curves of Aron, Hoffman, and Williams.[12] The extrapolated range is 95.5 gm/cm^2. Bakker and Segrè[13] have measured the extrapolated range of the electrostatically deflected proton beam to be 93.7 gm/cm^2. R. L. Mather[14] has independently determined the energy of the electrostatically deflected beam by means of the Cerenkov radiation in dense glass. He finds the energy to vary from 339 Mev to 341 Mev, depending upon the setting up of the deflecting system. Taking this as a correct value, and comparing the range with that of Bakker and Segrè, it is found that the energy of the scattered deflected beam may be as high as 344 Mev. It is expected that the scattered deflected beam may have a slightly higher energy than the electrostatically deflected beam, since its orbit must expand to a slightly greater radius than that at which the electrostatic deflector operates. Bakker and Segrè indicate that the curves of Aron, et al. give an energy which is slightly too low due to the fact that they used too high an ionization potential in their calculations. Since the ionization potential enters into the

---

12 W. A. Aron, B. G. Hoffman, and F. C. Williams, Range-Energy Curves, AECU-663

13 C. J. Bakker and E. Segrè, Phys. Rev. 81, 489 (1951)

14 R. L. Mather, Ph.D. dissertation, University of California (1951)

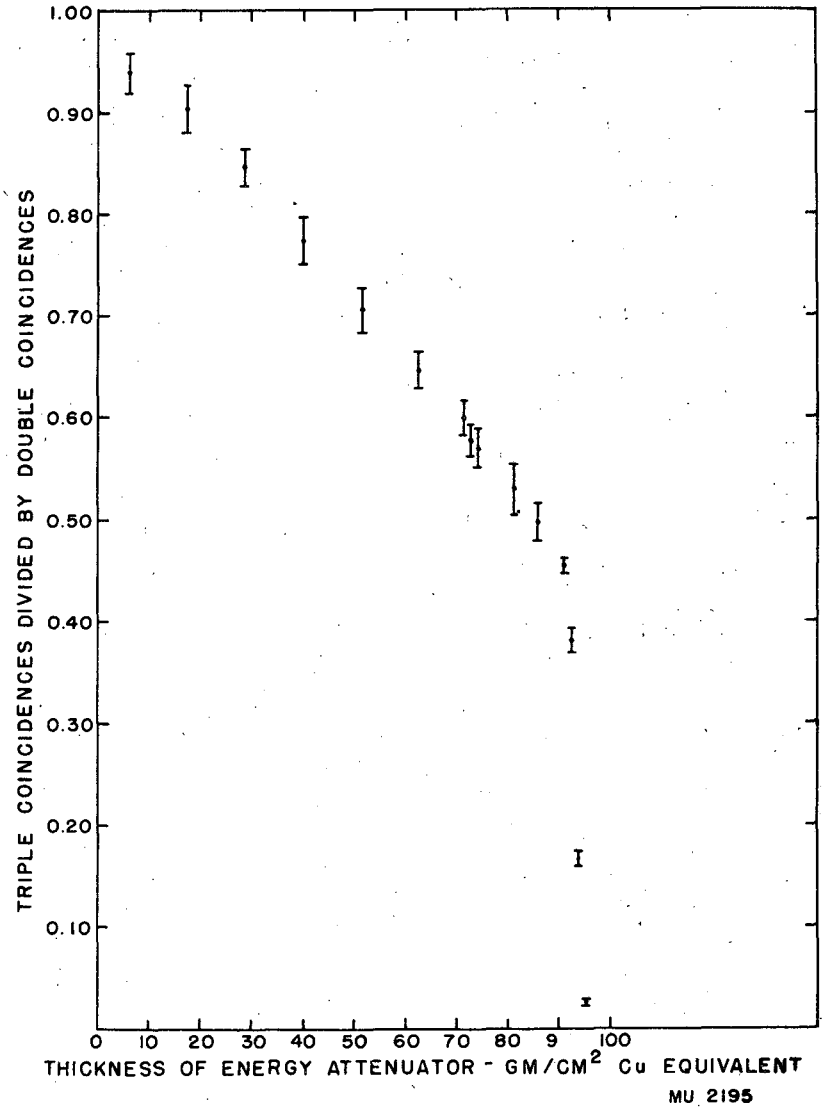
1.00
0.90
0.80
0.70
0.60
0.50
0.40
0.30
0.20
0.10
TRIPLE COINCIDENCES DIVIDED BY DOUBLE COINCIDENCES
0
10
20
30
40
50
60
70
80
9
100
THICKNESS OF ENERGY ATTENUATOR - GM/CM^2 Cu EQUIVALENT
MU 2195

Fig. 3

energy loss equation in a logarithmic term, the error is expected to be small, and the discrepancy between the range-energy curves and the measurements of Mather may be considered to be due to this error.

The detection efficiency, which is determined by reading the ratio corresponding to the thickness of energy attenuator used in the experiment, varies from 40 percent to 53 percent in the various runs, but is constant within a given run. In determining the energy threshold, the energy loss of the protons due to ionization in the target must be added to the ionization loss in the energy attenuator. The decrease in energy due to center of mass motion must also be considered, but is negligible except for the lightest target elements used. The decrease in the number of protons due to inelastic scattering in the target of particles which are also elastically scattered is negligible.

G. Lining Up the Scattering Table

The detection angle is determined by setting the pointer of the telescope arm at a particular marker on the calibrated angular scale of the scattering table. The 0° line is aligned with the proton beam in the following manner:

After the cyclotron has been tuned up and a satisfactory beam has been obtained in the cave, x-ray films are exposed in the beam at the front and rear of the cave. The developed films show darkened spots where the beam has passed through them. The centers of these spots are used to stretch a string through the cave in the position occupied by the beam center. Fiducial marks at the front and rear of the scattering table are then aligned with respect to this string, after which the string is removed and a film is exposed at the scatterer position as a check on the

alignment. With reasonable care, it is possible to align the table to within a small fraction of a degree.

IV MEASURING EQUIPMENT

A. Ionization Chamber and Beam Integrator

The proton beam is monitored with an argon-filled ionization chamber operated at a pressure of 92 cm Hg and with a sensitive thickness of 2.002 inches. The multiplication factor of the chamber has been measured by comparison with a Faraday cage and found to be 1095 ± 15 for 340 Mev protons. The chamber is operated at a voltage high enough so that there is no detectable ion recombination before collection.

The charge collected by the ionization chamber is stored in a standard capacitor whose voltage is continuously recorded upon moving paper tape by means of a Speedomax recorder fed from a feedback d.c. amplifier. The amplifier maintains its input grid at ground potential so that the leakage in the signal cable leading to the capacitor is negligible and the capacitance of the cable does not have to be considered in determining the total charge collected in terms of the recorded voltage. The recording circuit automatically recycles after attaining a predetermined voltage, so that the leakage is reduced since the capacitor is never charged to a very high voltage. The recording circuit automatically calibrates itself periodically against a standard cell.

B. Scatterers

The C, Al, Cu, Ni, and Pb scattering targets were machined from stock materials. The Ta and W targets were cut from stock foil. The S, Si, and Mg targets are pellets which were compressed from powdered

stocks. The Si targets contain a small amount of hydrocarbon binder. The Bi targets were cast. After forming, the targets were weighed on chemical balances and their dimensions measured with micrometer calipers. The weights and dimensions thus determined are used in the calculations. The densities were also calculated and compared with known densities to rule out the possibilities of "blow-holes" or voids.

C. Energy Attenuators

The energy attenuators are two inch square slabs of Cu machined from stock materials. They were weighed and measured in the same manner as were the scattering targets. Their densities were found to agree with the known density.

D. Proton Telescope

The scattered protons are detected by a triple-coincidence scintillation counter telescope consisting of three trans-stilbene crystals each viewed by a 1P21 electron photomultiplier tube. The signals from the photomultipliers are amplified, clipped, limited, and fed to the coincidence circuit. It is necessary to limit the amplitude of the pulses since the background includes a great number of inelastically scattered protons which are going slowly in the first two crystals, thus giving pulses very much larger than those due to the elastically scattered particles. These large pulses are apt to five feed-through unless all the pulses are limited to some standard height. The coincidence circuit is found to work most efficiently when all the pulses are of the order of two volts in amplitude.

Where they are not too high, the single and double coincidence counting rates are measured as a monitor of the operation of the equipment.

Angular resolution of the telescope is determined by the opening in a one-inch thick Cu collimator placed between the first and second phosphors. This thickness is sufficient so that any particle missing the opening will not be counted in the last crystal.

In order to decrease the individual counting rates the entire telescope is enclosed in a 1/4-inch thick Cu box to keep out the general background of slow particles which exists in the cave. In front of the first crystal is placed a three inch long Cu block having in it a hole of the same size as and aligned with the hole in the collimating block. It has been determined that the presence of this block appreciably decreases the single counting rates of the first and second phosphors, by keeping out randomly directed particles.

The first and second phosphors are made only slightly larger than the opening in the collimating block since the background counting rate is dependent upon the whole volume of the scintillators, while only the portion offered to the collimator is effective in giving true counts. The last crystal is made approximately an inch and a half square in order to count a large portion of the protons which are multiply scattered in the energy attenuating Cu blocks.

The stray magnetic field in the cave due to the cyclotron magnet is about 20 gauss. Since photomultipliers do not operate well in this field, the entire telescope is enclosed in a magnetic shield of one-eighth inch thick mild steel with a 1/4-inch thick lid. The magnetic shield has a hole in the front wall to allow the scattered protons to enter. The proton telescope is shown in Fig. 4.

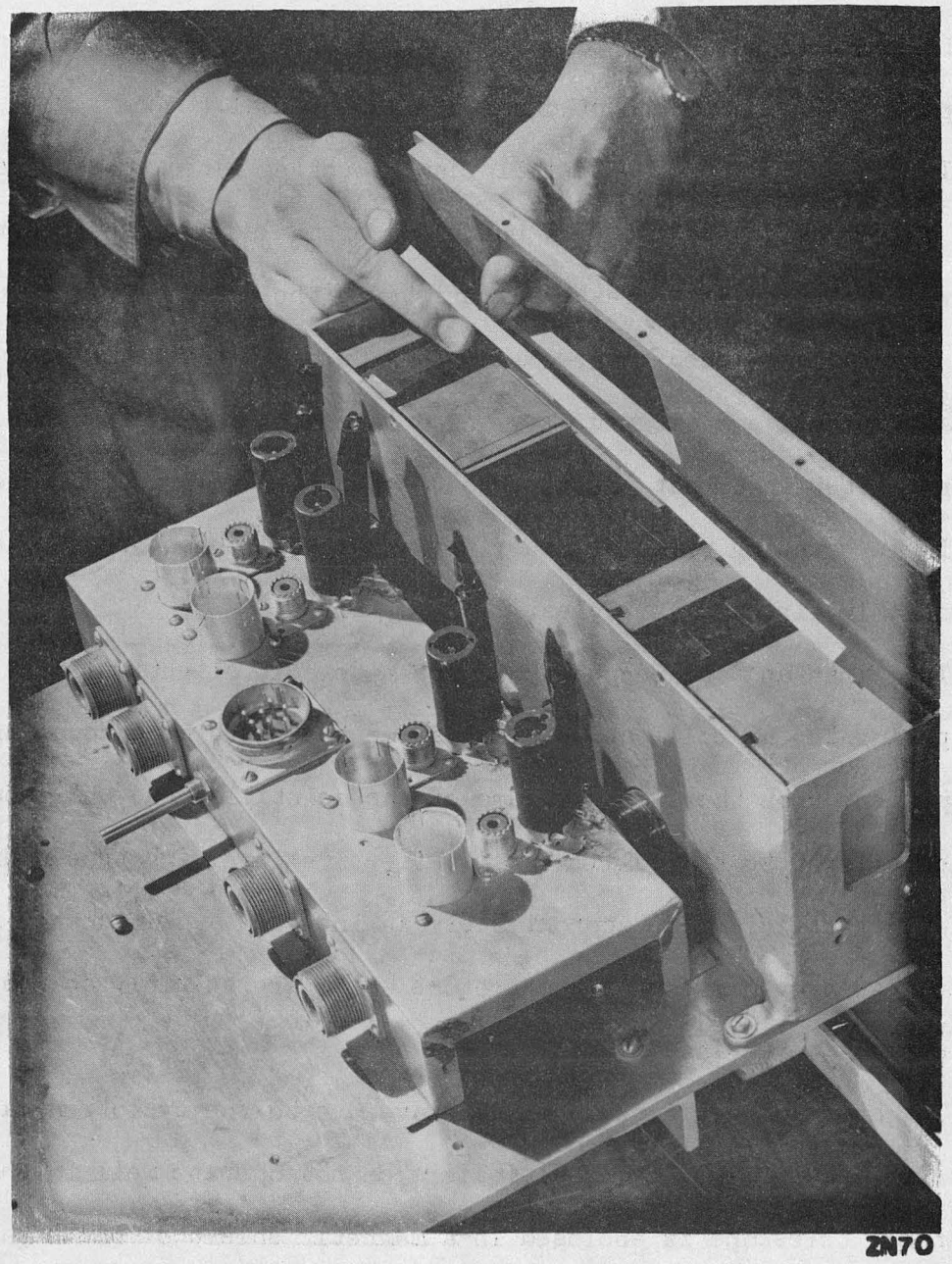

Fig. 4

E. Scattering Table

The proton scattering table is shown in Fig. 5. There are adjusting screws to adjust the vertical and horizontal position of the table during the lining-up process. The targets are mounted upon a remotely controlled hexagonal wheel allowing several targets to be run at the same scattering angle without necessitating a shut-down of the cyclotron in order to enter the cave. Pilot lights at the control station indicate which target is in the scattering position at any time.

The proton telescope is mounted on casters and is clamped to a rigid dural channel which keeps it pointed at the scatterer. This 56-inch long arm is pivoted by ball bearings upon the shaft which supports the scatterer wheel. At the outer end of the arm is a vernier scale which moves with it and is read with respect to 1° markers upon the table top.

In order that the target will always be set at half the angle at which the telescope is set, the scatterer support is connected to the telescope arm by means of an equal-arm pantograph, which insures the bisecting of the angle.

In order to take advantage of the line character of the scattered deflected beam after it was noticed, a tilting scattering frame was constructed. The geometry of scattering is the same as for the original scattering table, but the plane in which measurements are made may be tilted to make it perpendicular to the "line source" which the beam produces as it strikes the scatterer. This frame is shown in Fig. 6.

F. Angular Resolution

The angular resolution of the experiment is determined by the size of the beam at the scatterer and the distance to and size of the telescope

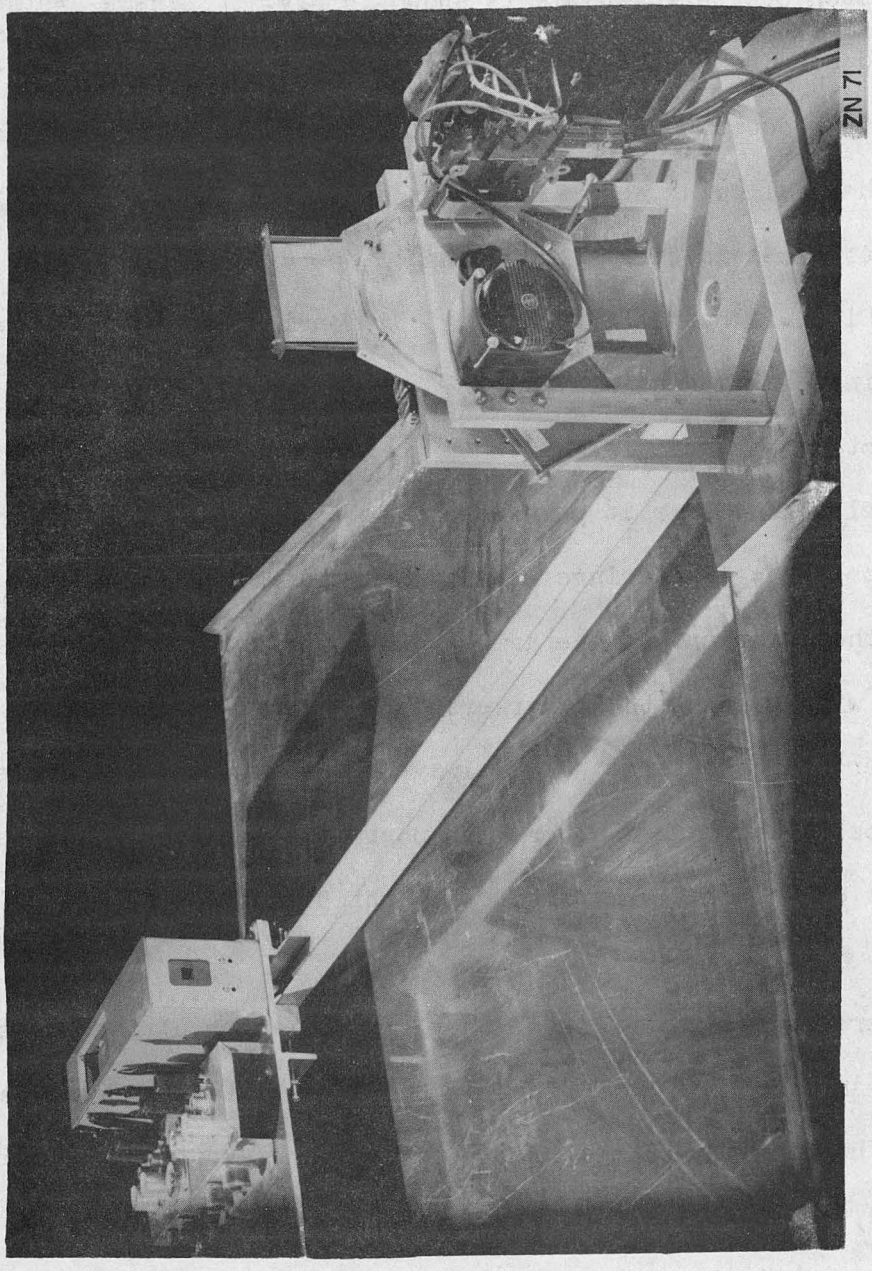

Fig. 5

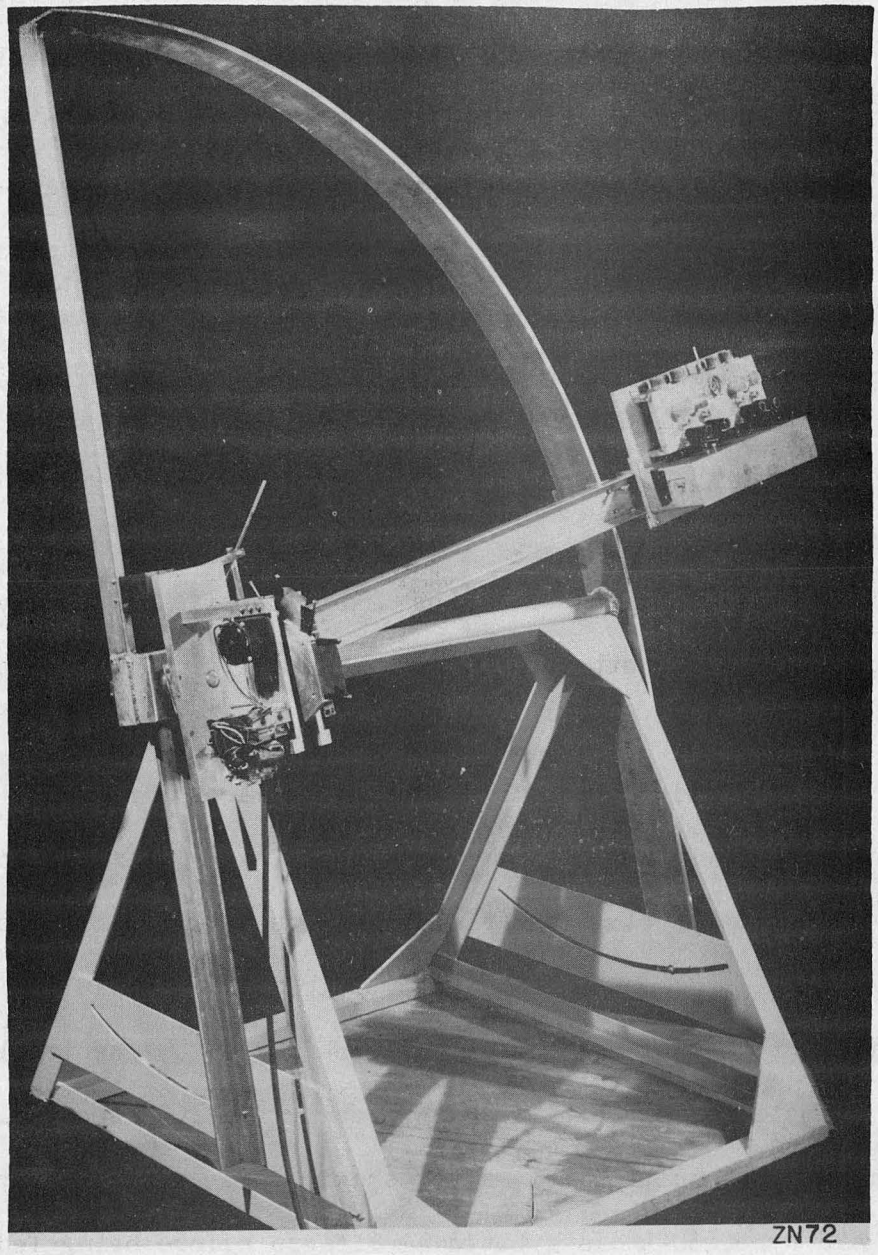

Fig. 6

collimator opening, as well as the angular divergence of the incident beam and the multiple Coulomb scattering in the scattering target. The thickness of the targets is so chosen that the mean square angle of multiple scattering in them is not greater than the desired angular resolution.

The total air path of the protons from the exit of the evacuated tube to the telescope is two meters. The root mean square displacement of 340 Mev protons in this path length is 1.8 mm. This displacement at the telescope would correspond to an angular spread of approximately $\pm$ 0.1°.

G. Coincidence Circuit

The coincidence circuit used in this experiment is a Rossi type quadruple coincidence circuit using a crystal diode as a diode clamp in the plate circuit, and a crystal diode signal expander circuit in the output. It was designed and constructed at this laboratory by R. Madey and B. Ragent for use in meson experiments, and is very similar to one constructed by Garwin.[15] In order to use this as a triple coincidence circuit, the signal from one of the photomultipliers is split and fed into two different channels of the coincidence circuit. The resolving time of the coincidence circuit is approximately 2×10^{-8} seconds. The signals from the photomultipliers, after shaping, are amplified by Hewlett-Packard type 460-A distributed amplifiers before being fed to the coincidence circuit. The coincidence output is fed through a linear amplifier to a scaler.

In order to insure that all of the protons scattered into the telescope are counted, a check is made of counting rate as a function of the

---

[15] R. L. Garwin, Rev. Sci. Instr. 21, 569 (1950)

photomultiplier tube supply voltage. As the voltage is increased it is expected that more of the weak pulses will be made large enough to cause counts. At excessively high tube voltages, the thermal noise level is expected to be so high as to give accidental coincidences. In Fig. 7 is shown a typical plot of triple coincidence counts per unit integrated beam as a function of tube voltage. It is seen that there is a very broad plateau in which all of the protons are being counted, but accidental coincidences are negligible.

V CALCULATIONS

A. Differential Scattering Cross Section

If the cross section does not vary appreciably over the angular region accepted by the telescope, at a given nominal angle, the number of true counts expected in the proton telescope when n protons are incident is given by

$$K(\theta) = Nn\, T_a\, T_s \frac{d\sigma}{d\Omega}(\theta)\, \Delta\Omega \qquad (11)$$

where:

N is the number of scattering nuclei per square centimeter, and is given by $N = \eta\rho x/A$ with ρx being the surface density of the scatterer in gm/cm^2, η Avogadro's number (6.023×10^{23}), and A the atomic mass number of the scattering material.

n is the number of incident protons, which is measured by the ionization chamber, and is equal to CV/ef, with C being the capacitance of the collecting capacitor, V the voltage to which the capacitor is charged, e the electronic charge (1.602×10^{-19}

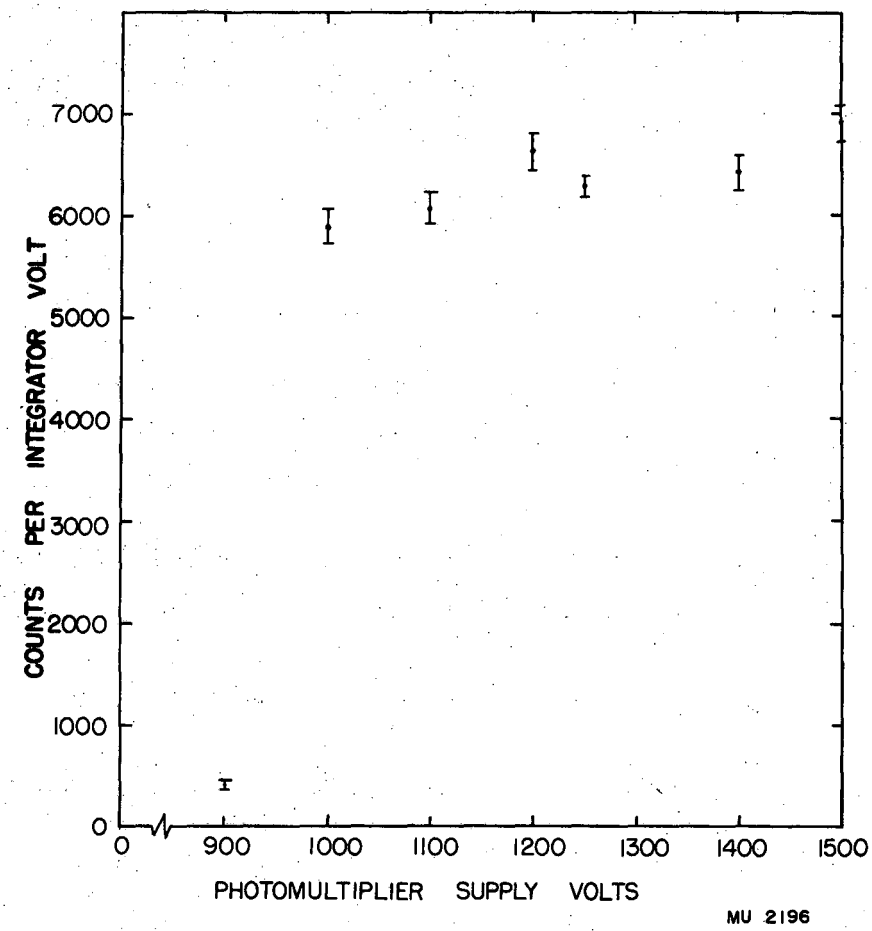
COUNTS PER INTEGRATOR VOLT
7000
6000
5000
4000
3000
2000
1000
0
0
900
1000
1100
1200
1300
1400
1500
PHOTOMULTIPLIER SUPPLY VOLTS
MU 2196

Fig. 7

coulombs), and f the multiplication factor of the ionization chamber.

T_a is the transmission factor of the energy attenuator and telescope, which is varied from 0.48 to 0.56 for the various runs.

T_s is the transmission factor of the scattering target.

$\Delta\Omega$ is the solid angle subtended by the proton telescope, $=S/a^2$, with S being the area of the opening in the collimating block and a the distance from the scatterer to the collimating block.

$\frac{d\sigma}{d\Omega}(\theta)$ is the differential elastic scattering cross section.

It must be noted that N varies as $(\cos 1/2\ \theta)^{-1}$ since the target is turned through $1/2\ \theta$.

Collecting all of the terms, and expressing the differential cross section in terms of measurable quantities and universal constants:

$$\frac{d\sigma}{d\Omega}(\theta) = \frac{K(\theta)}{\frac{\eta\rho x}{A}\ \frac{CV}{ef}\ T_a\ T_s\ \frac{S}{a^2}\ \frac{1}{\cos 1/2\ \theta}} \qquad (12)$$

For the purpose of calculation, the constants are collected, and calculated for use in each run, the formula used being:

$$\frac{d\sigma}{d\Omega}(\theta) = \frac{K(\theta)}{V}\ (\cos 1/2\ \theta)\ x\ (\text{constant}) \qquad (13)$$

The true counting rate is determined from the actual data by subtracting the background counts per integrator volt from the actual counts per integrator volt recorded during a datum run. The statistical deviation due to the counting statistics is the square root of the sum of the squares of the individual deviations of actual and background counts per volt.

B. Total Cross Section for Elastic Scattering

The total elastic scattering cross section is found by integrating the differential cross section over all angles. While the measurements do not give a true picture of nuclear scattering at extremely small angles due to Coulomb effects, the total solid angle included in these angles is very small and does not contribute much. As an approximation for the integration, the differential cross section curve is made to approach the zero degree axis in the same manner as was found in the 83 Mev neutron results of Bratenahl, et al.[2] The contributions at angles larger than those measured will be small but finite.

C. Angular Resolution

The angular resolution is determined by the geometry of the detection system and by the thickness of the scattering target. The size of the beam at the target, which determines the effective size of the source which the telescope sees, and the size of the opening in the telescope collimating block are so chosen that the maximum deviation from the nominal scattering angle at which a proton may be scattered and still be detected is equal to the nominal angular resolution. The angular deviation at which the intensity falls to half maximum is somewhat smaller than this. The angular spread due to multiple Coulomb scattering in the target is Gaussian, with the thickness of the target so chosen that the half-width at half maximum is equal to the nominal angular resolution.

The angular divergence of the incident beam is negligible in the determination of angular resolution due to the long path from the cyclotron to the cave. The main function of the collimators is to limit the size of the beam, with improvement of angular spread of the incident beam of secondary importance.

VI RESULTS AND CURVES

A. Angular Distributions

The data for the angular distributions for the elements measured are tabulated in Tables I through IV, and plotted in Figs. 8 through 21. The differential elastic scattering cross section in barns per steradian is shown as a function of the angle of scattering in the laboratory system, which is equivalent to the center of mass system except for large angles, where the difference is a few degrees for light elements. The center of mass angle is larger than the laboratory angle by 3.5° at 50° for C. The difference is only 1.6° for Al at 50°. It is correspondingly smaller for the heavier elements. The barn is the usual unit for cross section measurements, and is equal to 10^{-24} cm^2. The errors shown are the usual standard deviations based upon counting statistics.

Because of the large variation of the cross sections with angle, the cross section scale is made logarithmic in the curves. It is interesting to note that the ratio of the cross section of C at 5° to that at 50° is about 60,000. It should be noted that the data are not all plotted with the same scales.

All of the data having a given angular resolution for each angle for each target element are combined, but the results for different resolutions are given separately.

In Fig. 22 the positions of the maxima and minima of the measured diffraction patterns are plotted as a function of atomic mass number. The data is tabulated in Table V. It should be noted that these points may be fitted by an $A^{-1/3}$ line, which should be expected.

The curves shown are the predictions of the transparent nucleus

theory, using the constants appropriate to the neutron results. On the Al curve, the datum points of Bratenahl, et al. have been plotted, with the angle multiplied by 0.469, which is the ratio of the wavelengths in the two experiments.

B. Total Elastic Scattering Cross Sections

The total cross sections for "nuclear" elastic scattering are found by continuing the curves toward zero degrees in the same shape as was found in the neutron case by Bratenahl, et al. The resulting curves are then integrated to determine the total elastic scattering cross sections. The results are tabulated in Table VI.

TABLE I

Summary of differential elastic scattering cross section measurements having ± 1° angular resolution. The errors shown apply only to the relative magnitudes and do not include a possible 5 percent error in assigning absolute magnitude. The data are compounded from all of the runs made. Those values marked by an asterisk were measured in only one run, and are thus subject to more possible error than are those measured in several runs.

Angle in Degrees	Cu	Ag	Pb
5	9.51 ± 0.28*	17.24 ± 0.57*	33.8 ± 1.4*
6	6.915 ± 0.13	9.65 ± 0.39*	15.46 ± 0.60
$7\frac{1}{2}$	2.78 ± 0.07*		3.02 ± 0.28*
8	1.375 ± 0.028	1.312 ± 0.067	1.415 ± 0.098
10	0.302 ± 0.011	0.328 ± 0.015	1.231 ± 0.049
11	0.113 ± 0.011*		
12	0.1136 ± 0.0049	0.332 ± 0.015	0.328 ± 0.026
$12\frac{1}{2}$	0.146 ± 0.011*		0.381 ± 0.086*
13	0.1397 ± 0.0074*		
14	0.1258 ± 0.0039	0.1751 ± 0.0082	0.159 ± 0.017
15	0.1485 ± 0.0060		
16	0.0834 ± 0.0038	0.0739 ± 0.0051	0.157 ± 0.016
$17\frac{1}{2}$	0.0746 ± 0.0081*		0.196 ± 0.043*
18	0.0396 ± 0.0026	0.0521 ± 0.0045	0.0720 ± 0.0082
20	0.0204 ± 0.0011	0.0331 ± 0.0021	0.0546 ± 0.0048
22	0.0194 ± 0.0016*	0.0324 ± 0.0031*	0.0408 ± 0.0055*
25	0.0110 ± 0.0029*		
30	0.00312 ± 0.00066	0.0057 ± 0.0013*	0.0061 ± 0.0024

TABLE II

Summary of differential elastic scattering cross section measurements having ± 1/2° angular resolution. The errors shown apply only to the relative magnitudes and do not include a possible 5 percent error in assigning absolute magnitude. The data are compounded from all of the runs made. Those values marked by an asterisk were measured in only one run, and are thus subject to more possible error than are those measured in several runs.

Angle in Degrees	C	Mg*	Al	Si*
5	1.866 ± 0.016		2.61 ± 0.09*	
6	0.905 ± 0.019		2.137 ± 0.059*	
7	0.609 ± 0.013*		1.552 ± 0.054*	
7½	0.657 ± 0.015*			
8	0.531 ± 0.030*		1.194 ± 0.060*	
10	0.3095 ± 0.0056		0.543 ± 0.028*	
11	0.233 ± 0.013*		0.289 ± 0.015*	
12	0.179 ± 0.007*	0.2062 ± 0.0031	0.1749 ± 0.0029	0.2007 ± 0.0080
12½	0.180 ± 0.006*			
13	0.1253 ± 0.006*		0.104 ± 0.006*	
14	0.0956 ± 0.005*	0.0954 ± 0.0028	0.0553 ± 0.0018	0.0749 ± 0.0028
15	0.0635 ± 0.0025		0.0338 ± 0.003*	
16	0.0522 ± 0.0035*	0.0495 ± 0.0022	0.02623 ± 0.0009	0.0424 ± 0.0020
17		0.0343 ± 0.0019	0.0162 ± 0.0007*	0.0318 ± 0.0018
17½	0.0320 ± 0.0028*			
18	0.0260 ± 0.0025*	0.0315 ± 0.0015	0.0184 ± 0.0006	0.312 ± 0.0015
19	0.0194 ± 0.0009*	0.0292 ± 0.0014	0.0201 ± 0.0006	0.0319 ± 0.0017
20	0.0102 ± 0.0005	0.0244 ± 0.0011	0.01517 ± 0.00052	0.0248 ± 0.0011
21		0.01906 ± 0.00098	0.01318 ± 0.00047	0.02254 ± 0.0010
22		0.0168 ± 0.0011	0.01140 ± 0.00049	0.0182 ± 0.0011
23	0.00641 ± 0.0003*		0.0123 ± 0.001*	
24		0.01198 ± 0.00062	0.00781 ± 0.00036*	0.01201 ± 0.00062
27	0.00311 ± 0.0003*		0.0044 ± 0.0004*	
30	0.00143 ± 0.00022		0.00171 ± 0.00031*	
31	0.00090 ± 0.0002*		0.00157 ± 0.0003*	
35	0.000275 ± 0.0001*		0.00071 ± 0.0002*	
40	0.000302 ± 0.00008		0.000245 ± 0.00007	
50	0.000044 ± 0.00003*		0.000080 ± 0.00006	

TABLE III

Summary of differential elastic scattering cross section measurements having ± 1/2° angular resolution. The errors shown apply only to the relative magnitudes and do not include a possible 5 percent error in assigning absolute magnitude. The data are compounded from all runs made. Those values marked by an asterisk were measured in only one run, and thus are subject to more possible error than are those measured in several runs.

Angle in Degrees	S	Cu	Pb
6	1.736 ± 0.042*	5.248 ± 0.082	12.71 ± 0.25
7		3.029 ± 0.074	4.01 ± 0.20
8		1.431 ± 0.036	1.097 ± 0.076
9	0.543 ± 0.205*	0.601 ± 0.015	1.220 ± 0.055
10	0.390 ± 0.008	0.290 ± 0.010	1.254 ± 0.059
11		0.0782 ± 0.0054*	0.786 ± 0.035
12	0.0862 ± 0.0022	0.0743 ± 0.0047	0.3028 ± 0.023
12½			0.203 ± 0.054
13	0.0411 ± 0.0020	0.0851 ± 0.0041*	0.125 ± 0.017*
14	0.0255 ± 0.0011	0.1083 ± 0.0052	0.083 ± 0.017
15	0.01017 ± 0.00073	0.0895 ± 0.0025	0.1011 ± 0.010
15½	0.0115 ± 0.0010*		
16	0.0097 ± 0.0012*	0.0673 ± 0.0031*	0.0939 ± 0.0094*
17	0.01418 ± 0.00070	0.0502 ± 0.0030*	0.0737 ± 0.0096*
18	0.01224 ± 0.00082		
19	0.0116 ± 0.0008*	0.0181 ± 0.0015*	0.0390 ± 0.006

TABLE IV

Summary of differential elastic scattering cross section measurements having high angular resolutions. The errors shown apply only to the relative magnitudes and do not include a possible 5 percent error in assigning absolute magnitude. These data are for a single run. Angular resolution is indicated for each value as follows: a, 1/8°; b, 1/5°; c, 1/4°; d, 3/8°; e, 1/2°.

Angle in Degrees	Ta	W	Pb	Bi
2.5	505 ± 27a	506 ± 30a	970 ± 37b	772 ± 19c
3	162.0 ± 8.6a	159 ± 13a	185 ± 12b	196.0 ± 8.5c
4	55.9 ± 3.9a	51.0 ± 3.8a	63.5 ± 3.8b	64.3 ± 2.8c
5	21.8 ± 1.8a	21.2 ± 1.9a	24.4 ± 2.2b	23.97 ± 0.82c
6	6.33 ± 0.93a	7.76 ± 1.1a	7.91 ± 0.92b	7.65 ± 0.52c
7			2.71 ± 0.53c	2.10 ± 0.46c
7.5	1.166 ± 0.096d	1.127 ± 0.079d	0.69 ± 0.30c	0.75 ± 0.29c
8			1.04 ± 0.30c	0.99 ± 0.26c
8.5	0.66 ± 0.11d	0.74 ± 0.10d	0.98 ± 0.45c	0.97 ± 0.41c
8.7	0.742 ± 0.086d	0.708 ± 0.075d		
9	0.728 ± 0.080d	0.811 ± 0.074d	1.15 ± 0.38c	1.64 ± 0.24c
9.5	0.786 ± 0.092d	0.641 ± 0.099d	0.94 ± 0.36c	0.96 ± 0.32c
10	0.806 ± 0.090d	0.866 ± 0.082d	1.19 ± 0.35c	1.40 ± 0.25c
11	0.571 ± 0.074d	0.541 ± 0.065d		0.32 ± 0.20c
12.5	0.290 ± 0.049d	0.289 ± 0.060d	0.203 ± 0.054e	0.198 ± 0.058e

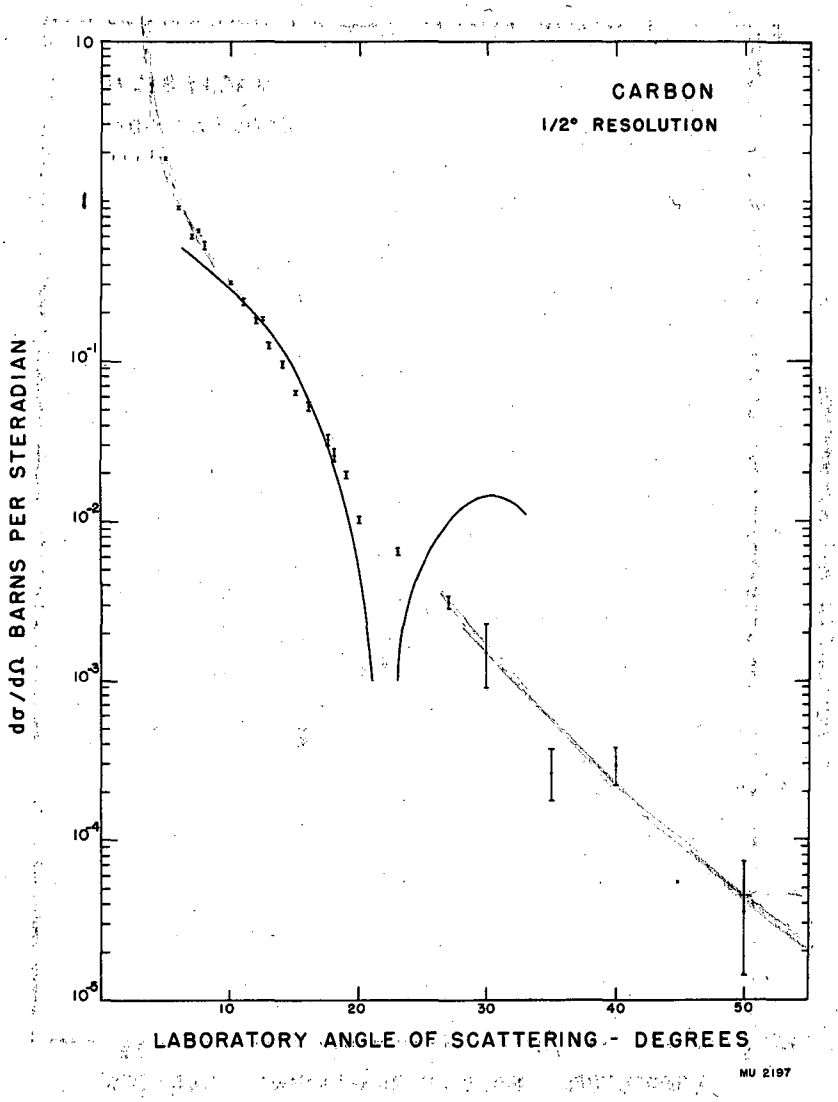
CARBON
1/2° RESOLUTION
dσ/dΩ BARNS PER STERADIAN
LABORATORY ANGLE OF SCATTERING - DEGREES
MU 2197

Fig. 8

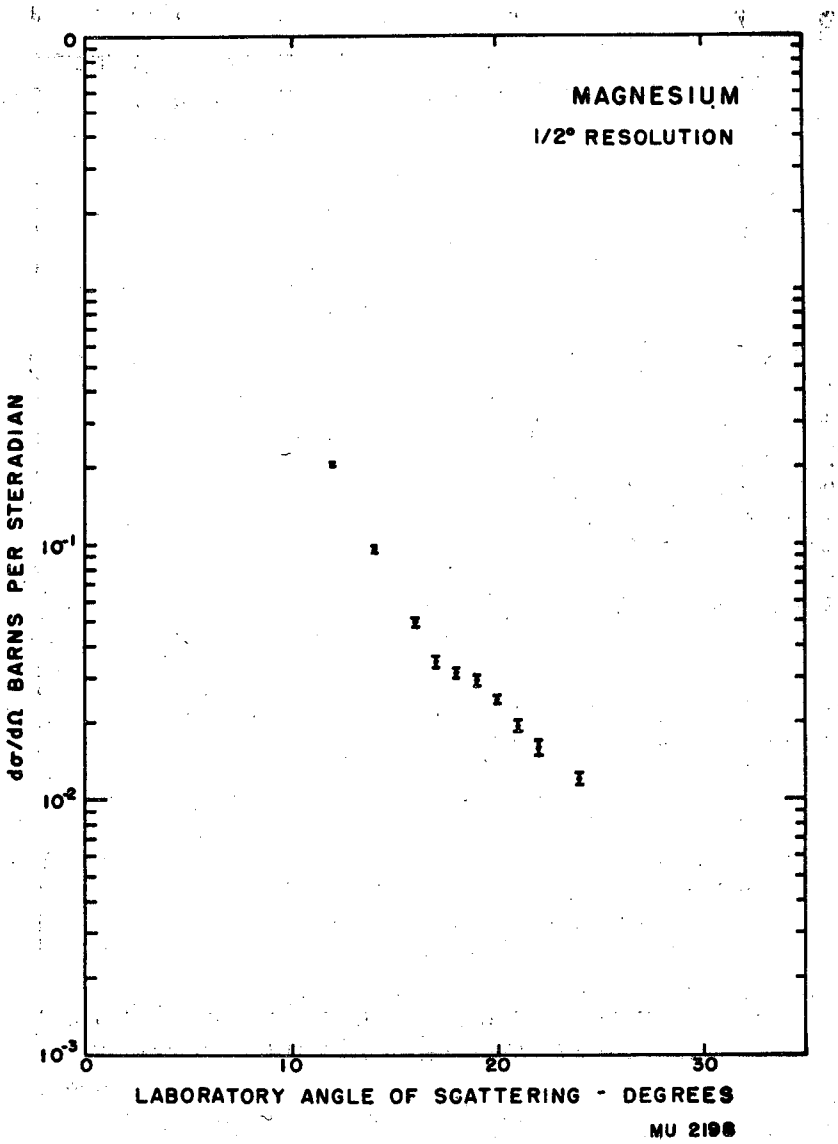
MAGNESIUM
1/2° RESOLUTION
dσ/dΩ BARNS PER STERADIAN
0
10⁻¹
10⁻²
10⁻³
0
10
20
30
LABORATORY ANGLE OF SCATTERING - DEGREES
MU 2198

Fig. 9

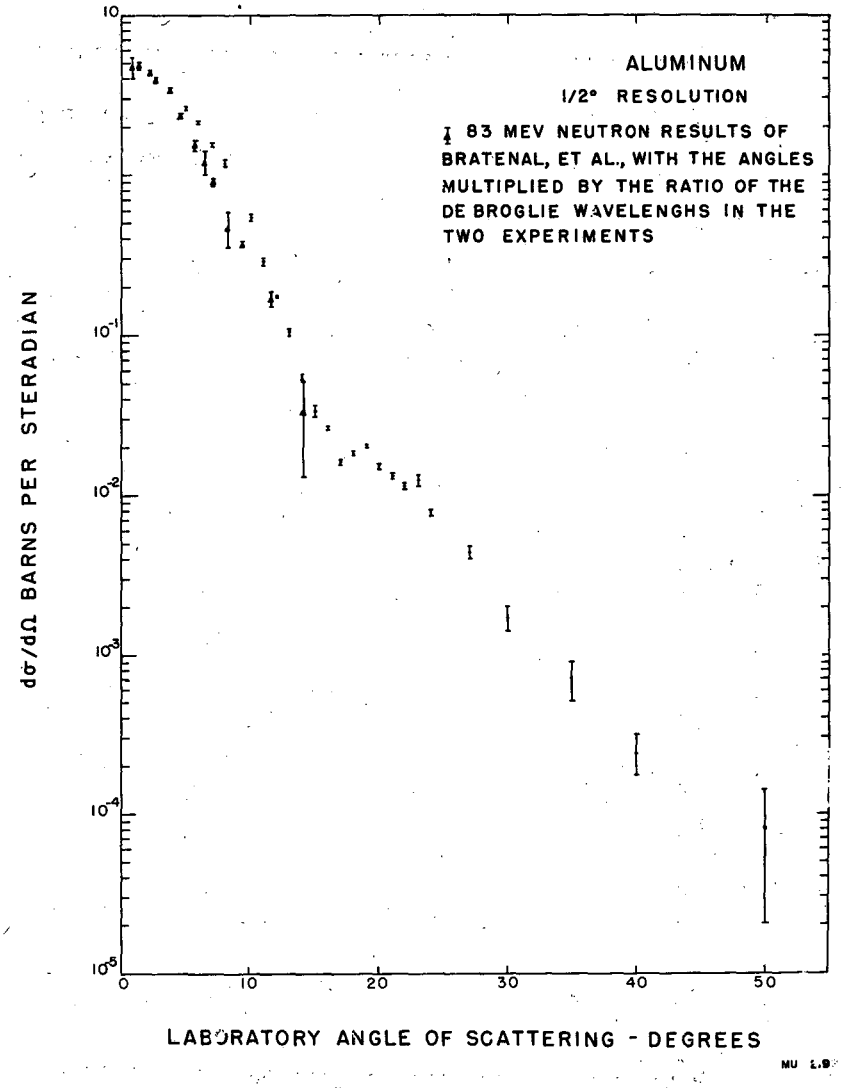
ALUMINUM
1/2° RESOLUTION
83 MEV NEUTRON RESULTS OF BRATENAL, ET AL., WITH THE ANGLES MULTIPLIED BY THE RATIO OF THE DE BROGLIE WAVELENGHS IN THE TWO EXPERIMENTS
dσ/dΩ BARNS PER STERADIAN
LABORATORY ANGLE OF SCATTERING - DEGREES
10
10⁻¹
10⁻²
10⁻³
10⁻⁴
10⁻⁵
0
10
20
30
40
50

Fig. 10

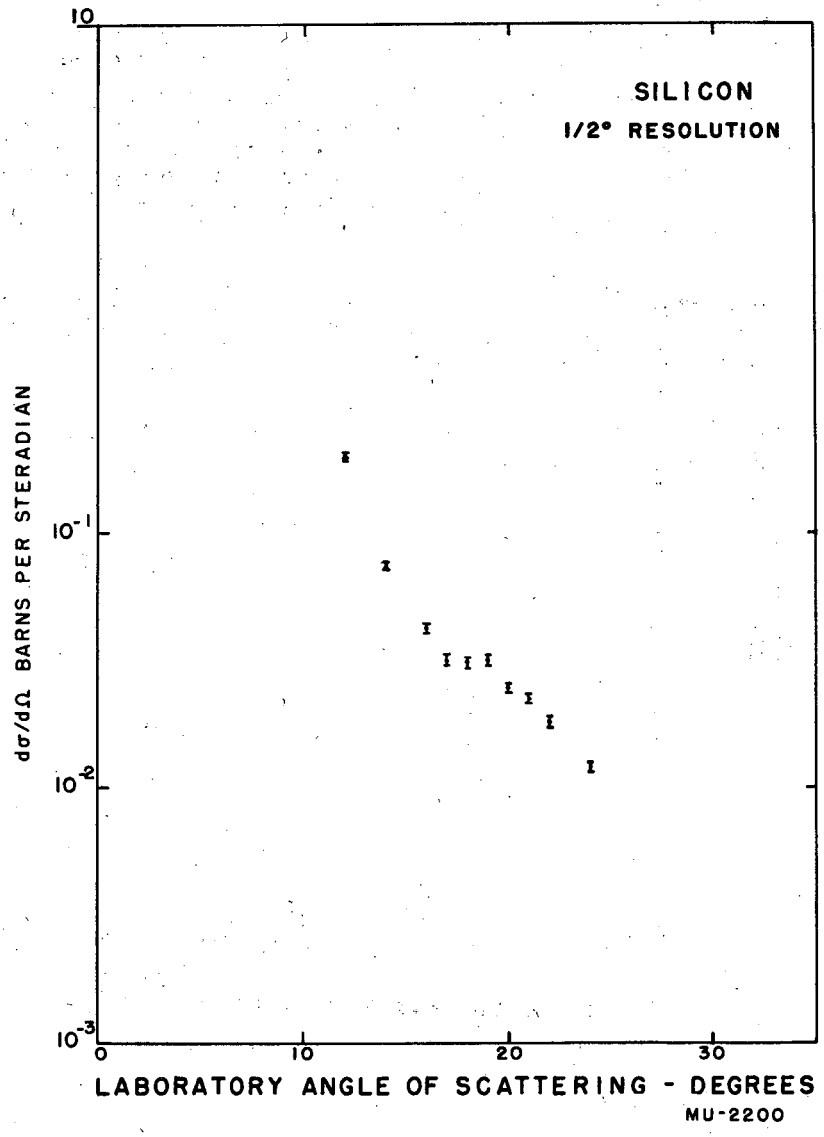
SILICON
1/2° RESOLUTION
10
10^{-1}
10^{-2}
10^{-3}
dσ/dΩ BARNS PER STERADIAN
0
10
20
30
LABORATORY ANGLE OF SCATTERING - DEGREES
MU-2200

Fig. 11

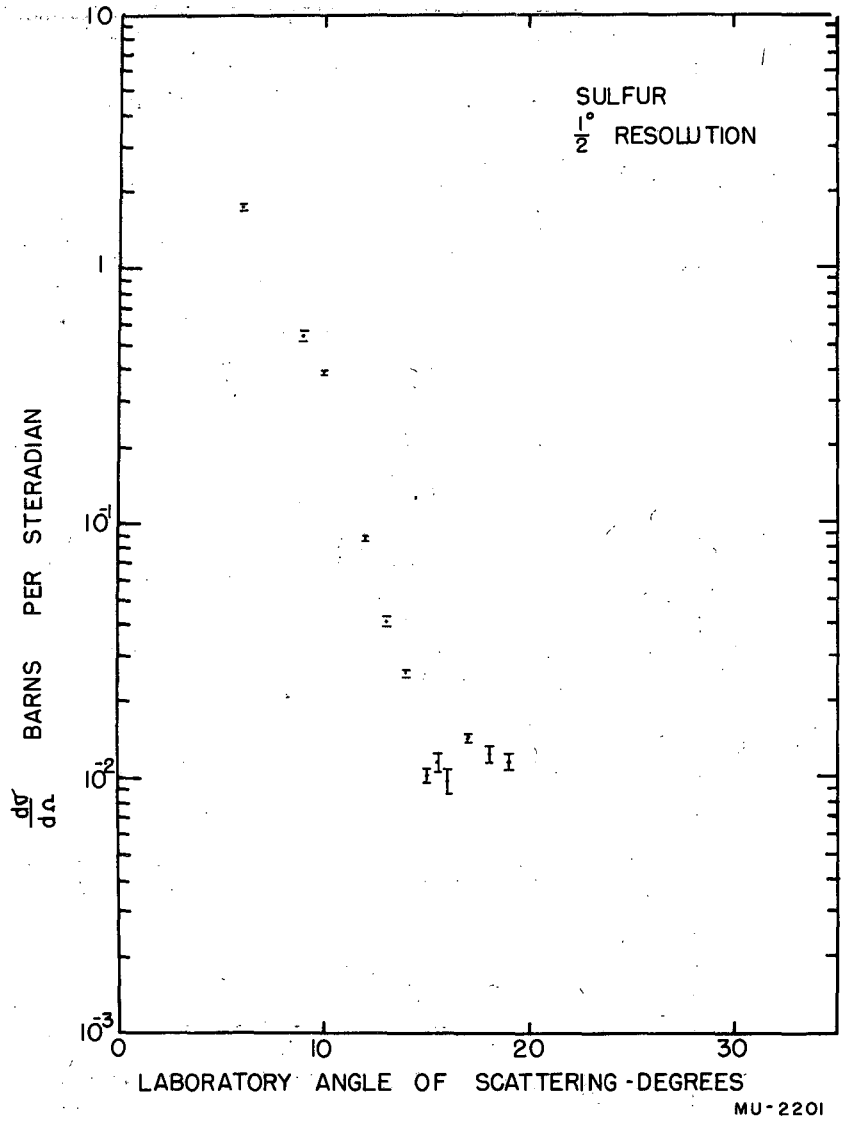
SULFUR
1/2° RESOLUTION
10
1
10⁻¹
10⁻²
10⁻³
dσ/dΩ BARNS PER STERADIAN
0
10
20
30
LABORATORY ANGLE OF SCATTERING - DEGREES
MU-2201

Fig. 12

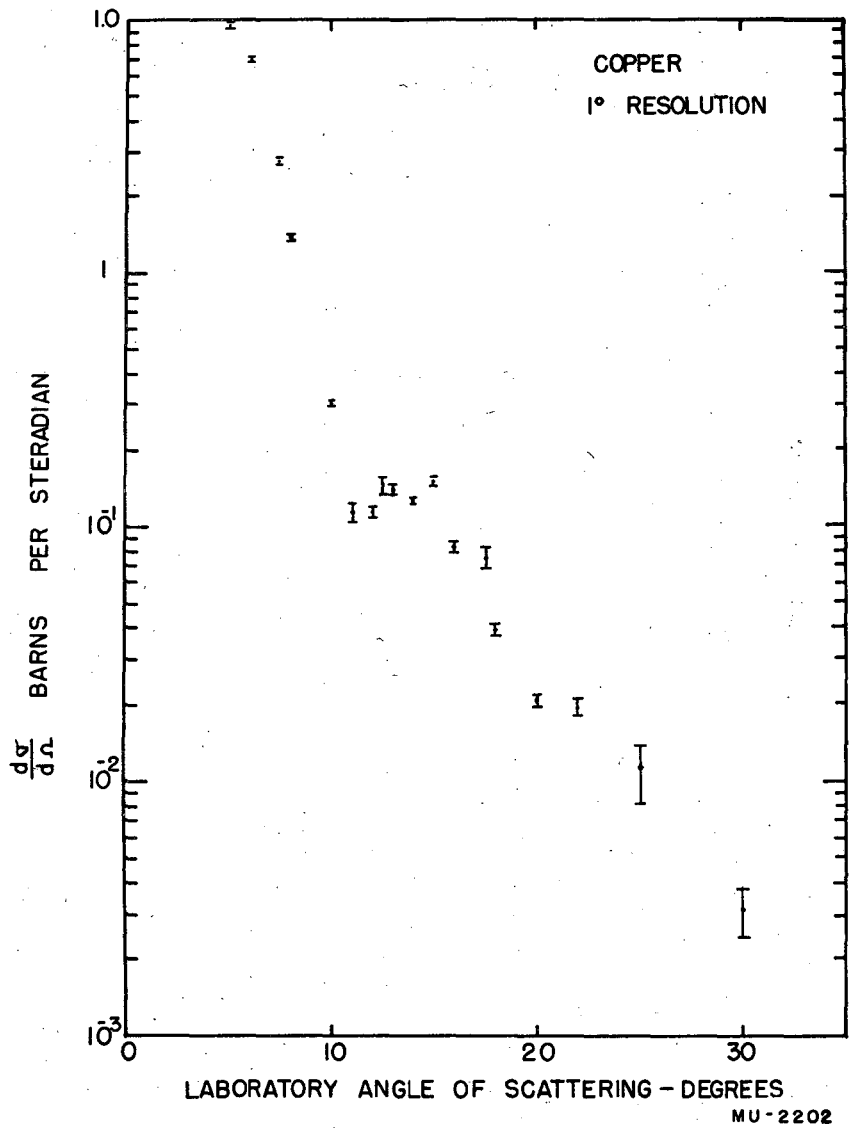
COPPER
1° RESOLUTION
1.0
1
10^{-1}
10^{-2}
10^{-3}
$\frac{d\sigma}{d\Omega}$ BARNS PER STERADIAN
0
10
20
30
LABORATORY ANGLE OF SCATTERING - DEGREES
MU-2202

Fig. 13

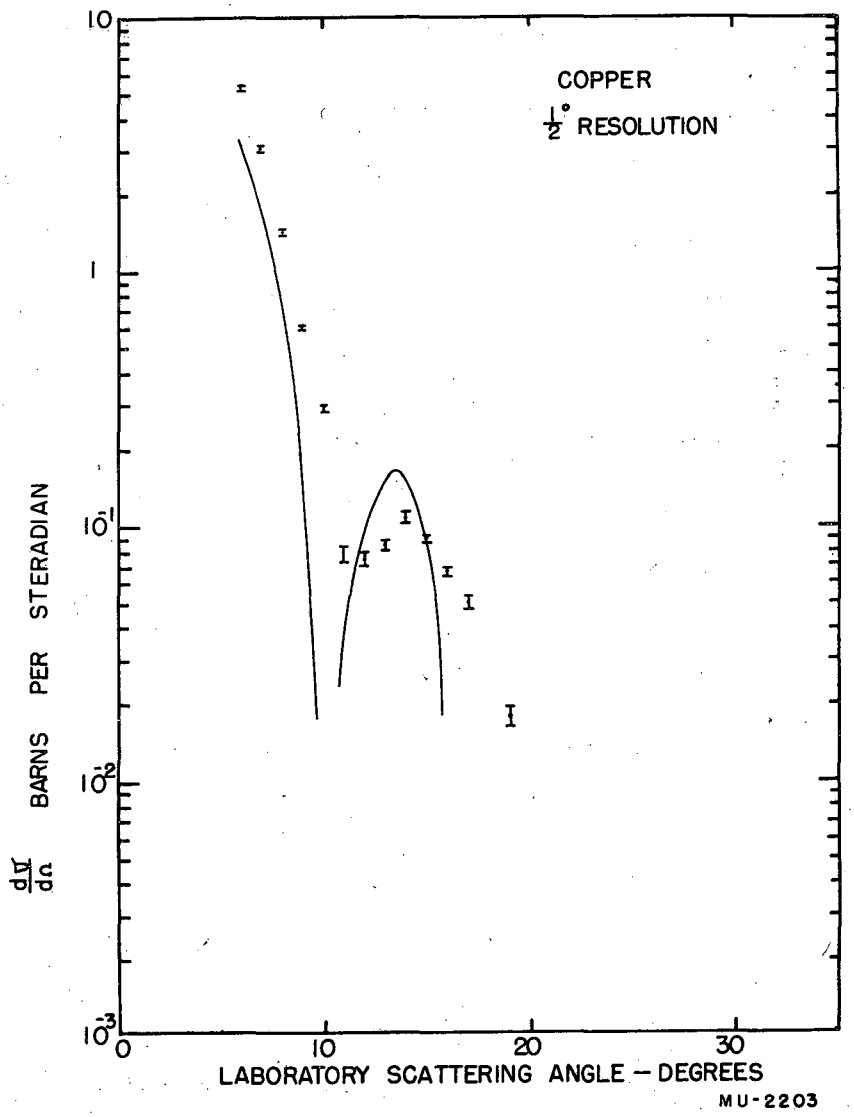
COPPER
½° RESOLUTION
10
1
10⁻¹
10⁻²
10⁻³
dσ/dΩ BARNS PER STERADIAN
0
10
20
30
LABORATORY SCATTERING ANGLE – DEGREES
MU-2203

Fig. 14

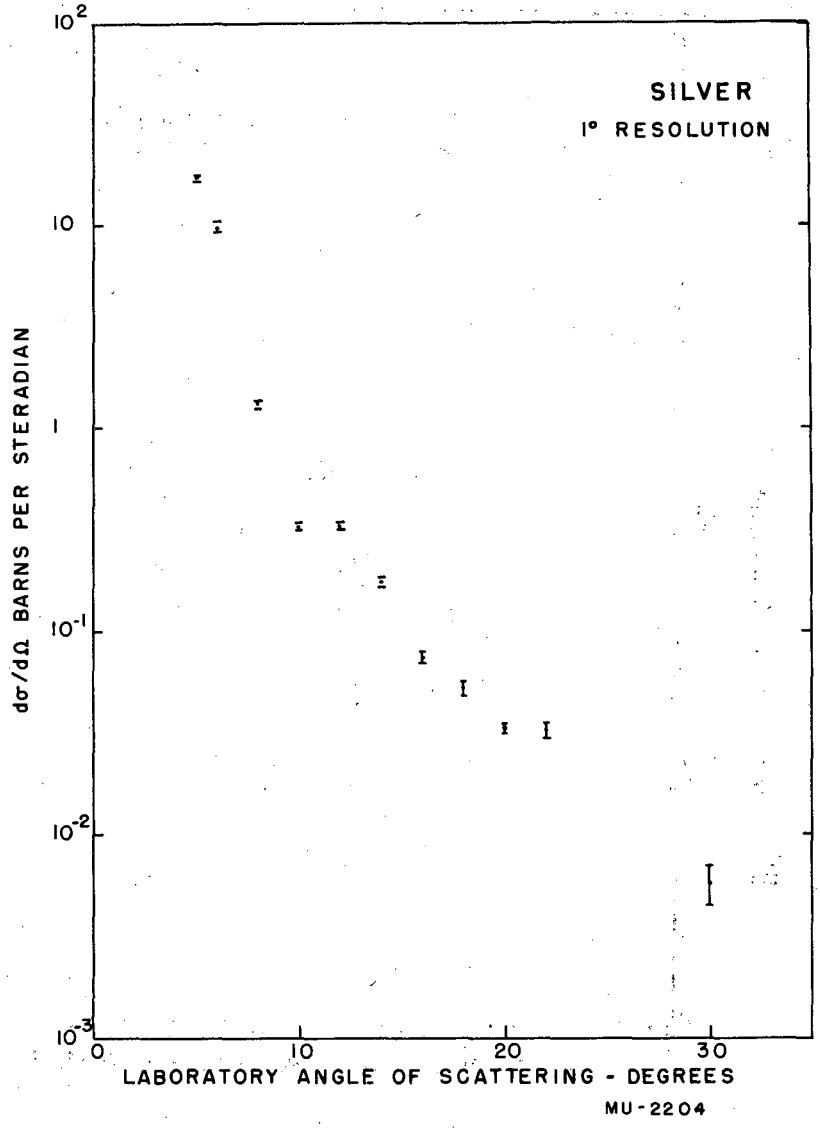
SILVER
1° RESOLUTION
10^2
10
1
10^{-1}
10^{-2}
10^{-3}
dσ/dΩ BARNS PER STERADIAN
0
10
20
30
LABORATORY ANGLE OF SCATTERING - DEGREES
MU-2204

Fig. 15

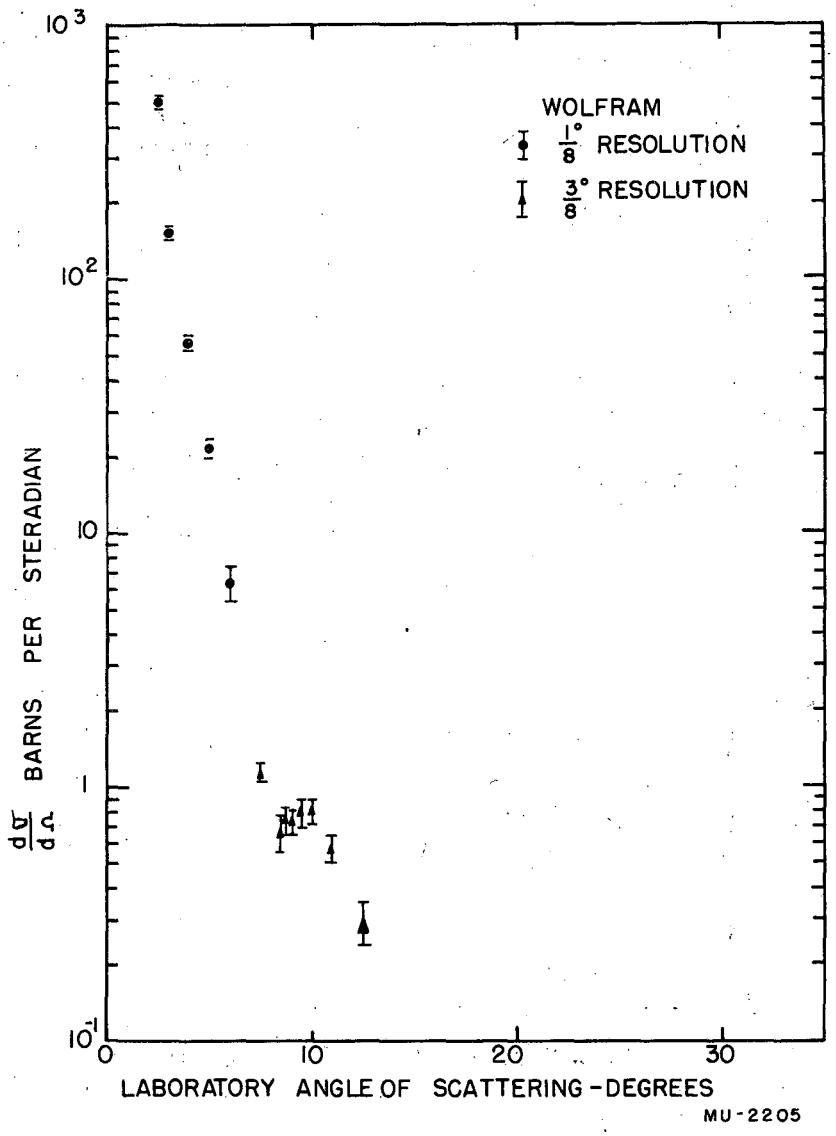
WOLFRAM
1°/8 RESOLUTION
3°/8 RESOLUTION
10³
10²
10
1
10⁻¹
0
10
20
30
dσ/dΩ BARNS PER STERADIAN
LABORATORY ANGLE OF SCATTERING - DEGREES
MU-2205

Fig. 16

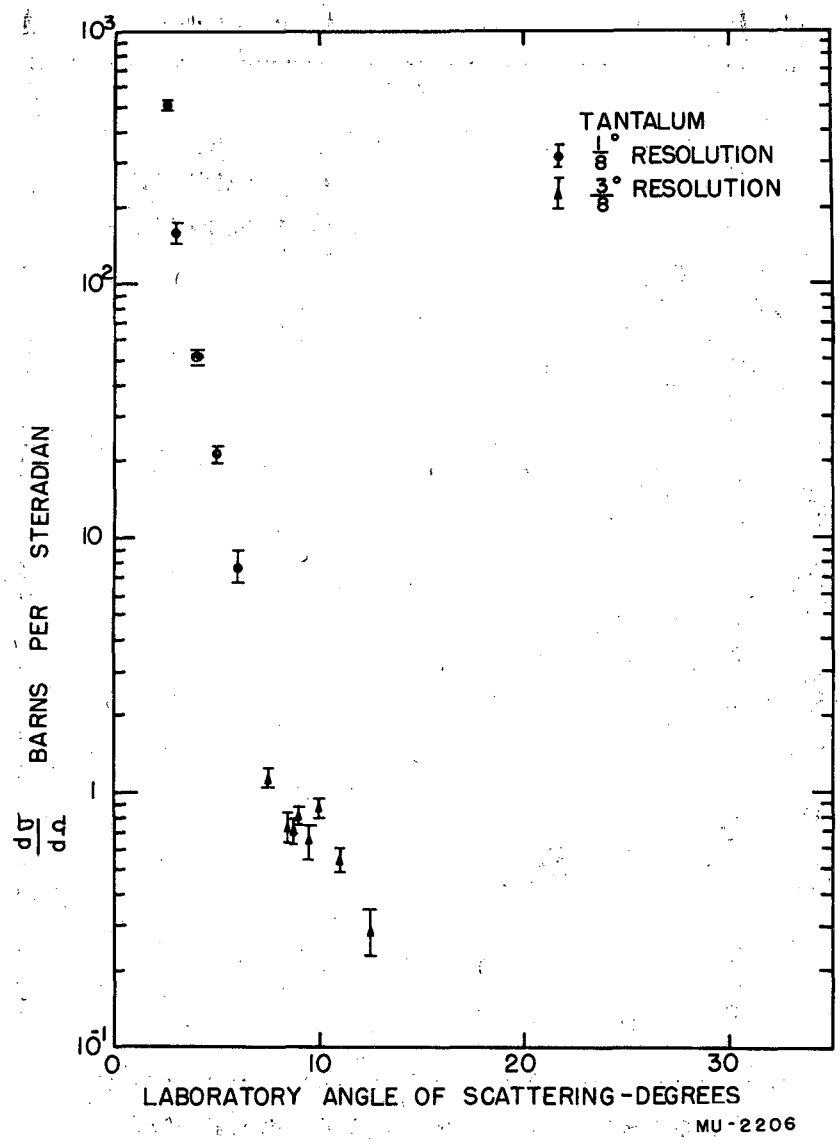
TANTALUM
1° RESOLUTION
3° RESOLUTION
10^3
10^2
10
1
10^{-1}
$\frac{d\sigma}{d\Omega}$ BARNS PER STERADIAN
0
10
20
30
LABORATORY ANGLE OF SCATTERING - DEGREES
MU-2206

Fig. 17

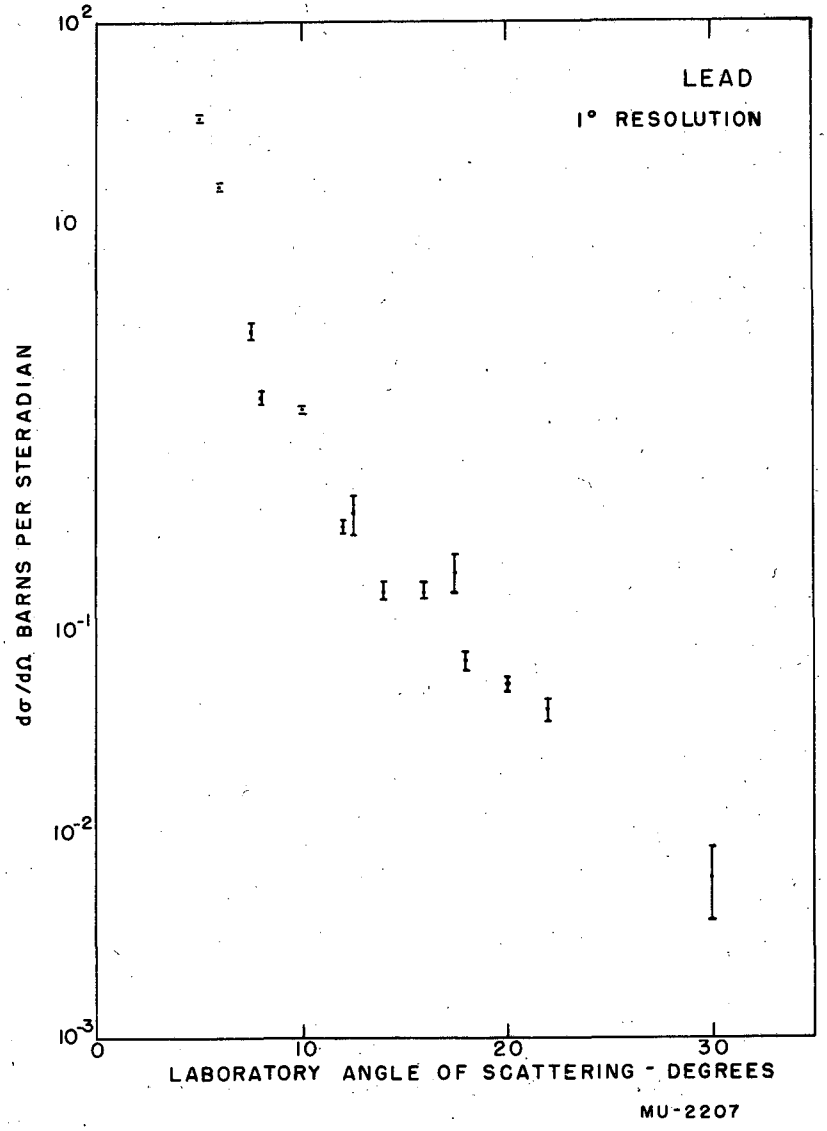
LEAD
1° RESOLUTION
10^2
10
10^{-1}
10^{-2}
10^{-3}
dσ/dΩ BARNS PER STERADIAN
0
10
20
30
LABORATORY ANGLE OF SCATTERING - DEGREES
MU-2207

Fig. 18

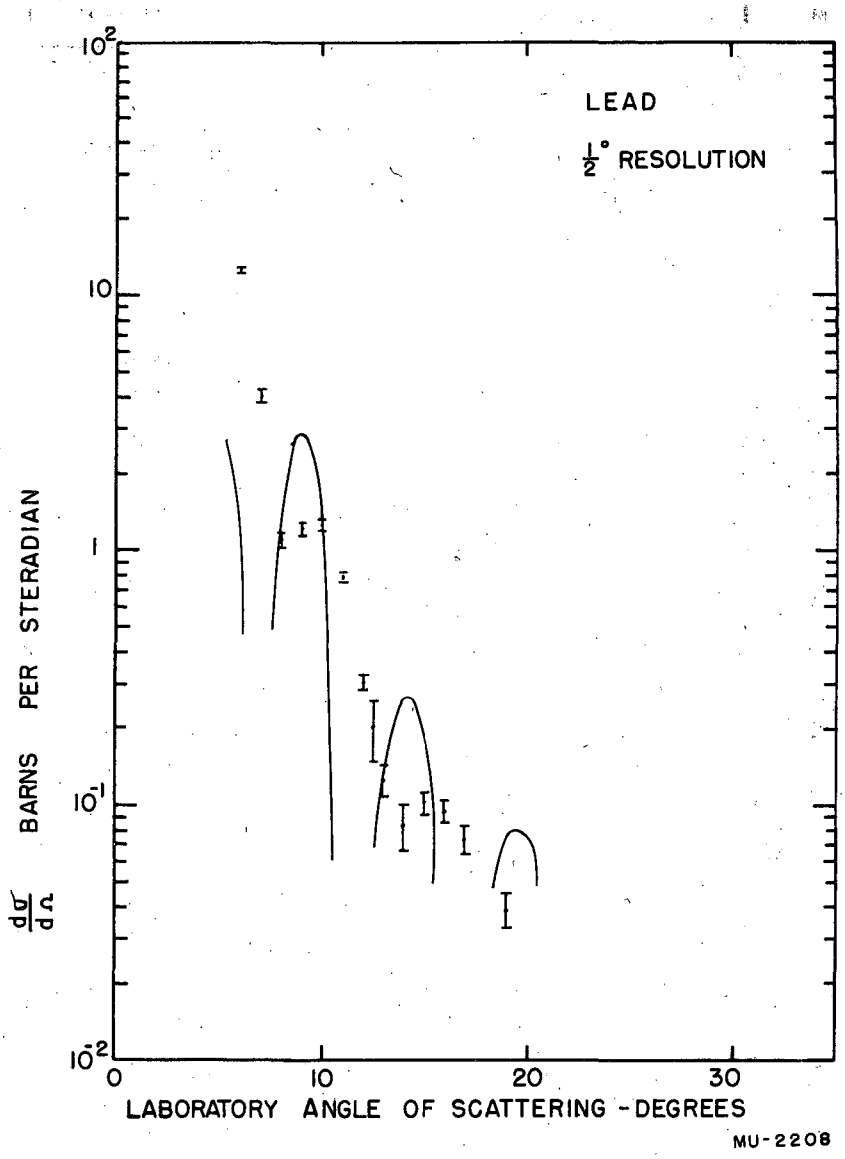
LEAD
½° RESOLUTION
10^2
10
1
10^{-1}
10^{-2}
$\frac{d\sigma}{d\Omega}$ BARNS PER STERADIAN
0
10
20
30
LABORATORY ANGLE OF SCATTERING - DEGREES
MU-2208

Fig. 19

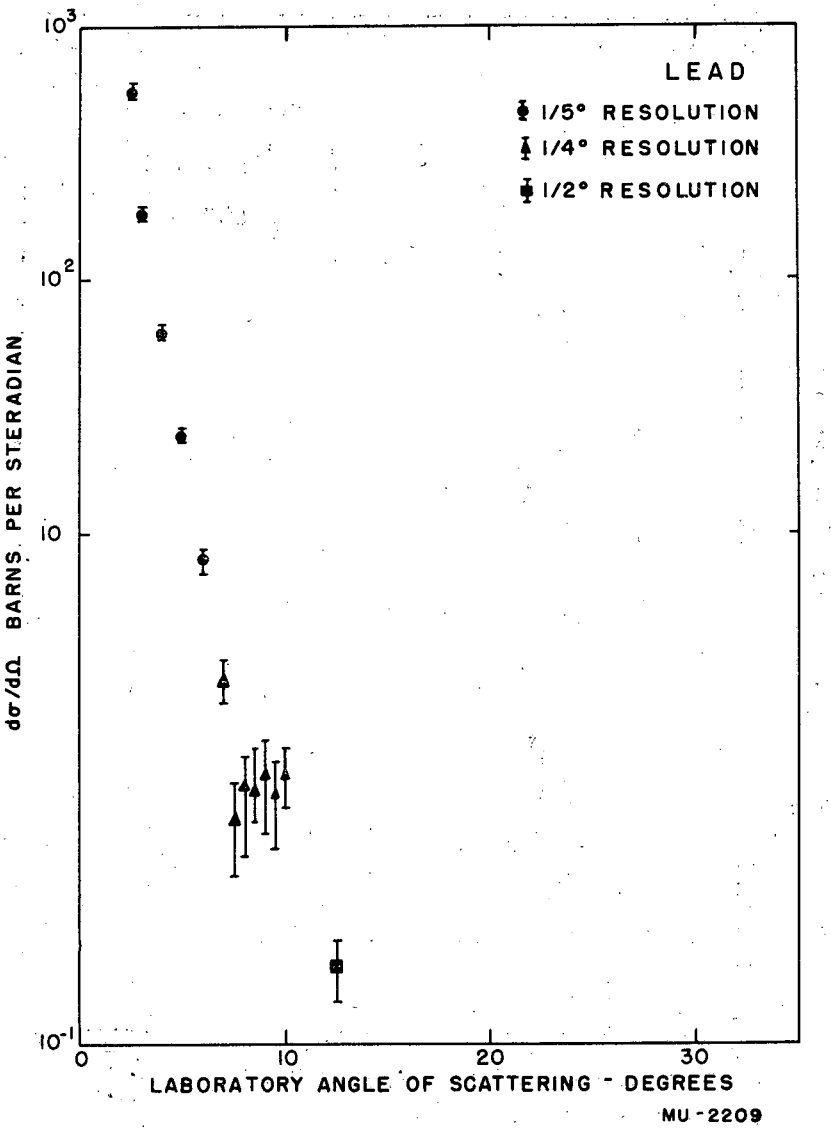
LEAD
1/5° RESOLUTION
1/4° RESOLUTION
1/2° RESOLUTION
10^3
10^2
10
10^{-1}
dσ/dΩ BARNS PER STERADIAN
0
10
20
30
LABORATORY ANGLE OF SCATTERING - DEGREES
MU-2209

Fig. 20

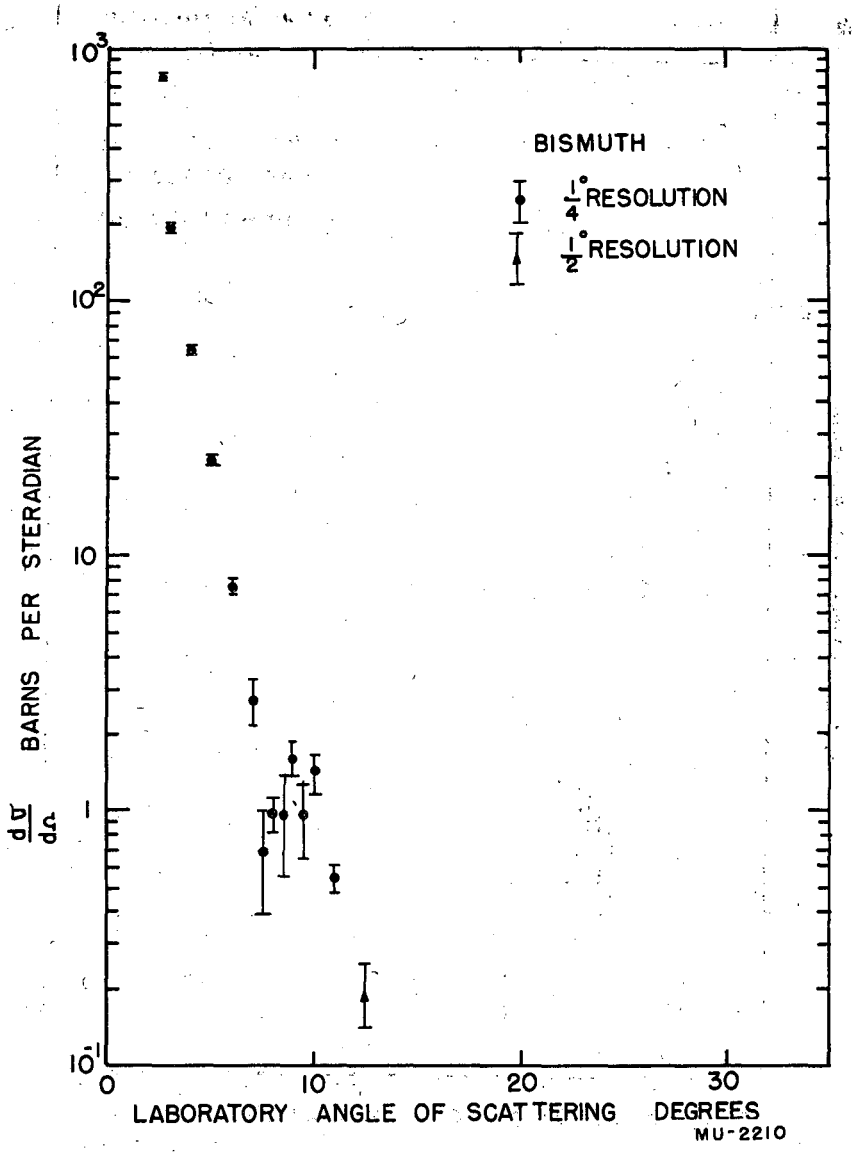
BISMUTH
1/4° RESOLUTION
1/2° RESOLUTION
dσ/dΩ BARNS PER STERADIAN
LABORATORY ANGLE OF SCATTERING DEGREES
MU-2210

Fig. 21

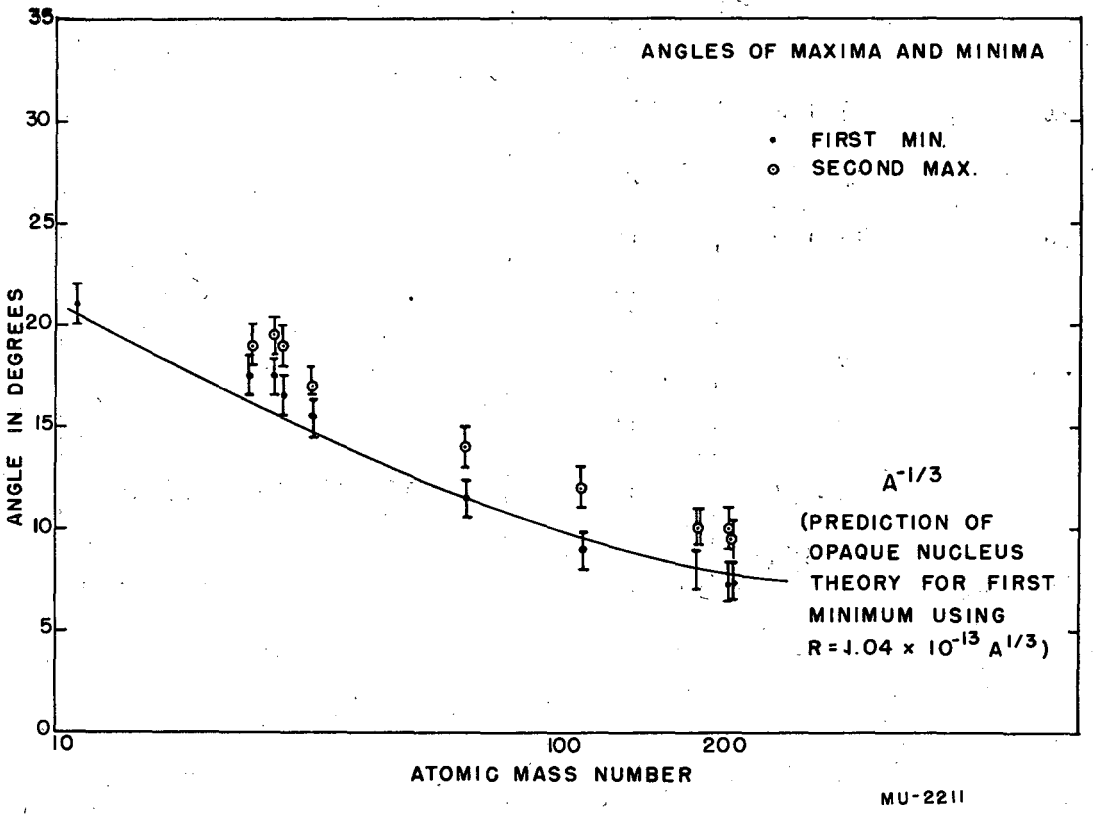
ANGLES OF MAXIMA AND MINIMA
• FIRST MIN.
⊙ SECOND MAX.
$A^{-1/3}$
(PREDICTION OF OPAQUE NUCLEUS THEORY FOR FIRST MINIMUM USING $R = 1.04 \times 10^{-13} A^{1/3}$)
ANGLE IN DEGREES
ATOMIC MASS NUMBER
0
5
10
15
20
25
30
35
10
100
200
MU-2211

Fig. 22

TABLE V

ANGLES OF MAXIMA AND MINIMA

Element	1st Min.	2nd Max.	2nd Min.	3rd Max.
C	21 (?)			
Mg	17-1/2	19		
Al	17-1/2	19-1/2		
Si	17-1/2	19		
S	15-1/2	17		
Cu	11-1/2	14		
Ag	9	12		
W	8	10		
Ta	8	10		
Pb	7-1/4	10	13-1/2	15-1/2
Bi	7-1/4	9-1/2		

TABLE IV

TOTAL CROSS SECTIONS FOR "NUCLEAR" ELASTIC SCATTERING

No errors are indicated, since the value is very sensitive to the method of continuing the differential cross sections toward zero degrees. In some cases, the use of the datum points at very small angles instead of neglecting the Coulomb scattering by continuing the curves to match the corresponding neutron data would change the cross section by a factor of 2 or 3. It should be emphasized that the curves were continued and the integration done systematically without regard to the expected answer. Tabulated for comparison are the total cross sections and the ratio of inelastic to total for 270 Mev neutrons as given by DeJuren[16] and by DeJuren and Moyer.[8]

Element	Cross Section (This Experiment)	Total Cross Section (Neutrons)	Ratio of Inelastic to Total (neutrons)
C	0.098	0.288 ± 0.003	0.505 ± 0.02
Al	0.201	0.555 ± 0.008	
Cu	0.515	1.145 ± 0.0015	0.51 ± 0.02
Ag	0.884		
Pb	0.934	2.84 ± 0.03	0.50 ± 0.01 (av)

16 James DeJuren, Phys. Rev. 80, 27 (1950)

VII SOURCES OF ERROR

A. Inhomogeneous Beam

It might appear that the method of removing the protons from the cyclotron by scattering them into the magnetic deflector would give a spread in the energy spectrum. Actually, the magnetic deflecting channel itself forms an efficient momentum selector.

The beam is contaminated by low energy protons due to inelastic scattering processes in the walls of the collimators and the ionization chamber. Most of these low energy protons are removed by the beam focusing magnet since the major portion of the collimation takes place in the pre-magnet collimator. The lower energy particles will not be counted as coincidences, but they will contribute to the total charge collected by the ionization chamber. The number of such particles present is small in comparison to the number of 340 Mev protons present.

B. Uncertainty in the Number of Particles

Besides the low energy particles which contribute to the uncertainty in the number of incident particles, there are other sources of uncertainty. For an intense beam there is apt to be recombination of ions in the ionization chamber before the ions can migrate to the plates to be collected. The integrated charge collected by the ionization chamber has been measured against a Faraday cage as a function of chamber collecting voltage. The chamber is operated in a voltage region in which the number of ions recombining is negligible.

During a long integrating period, there is a possibility that some of the collected charge may leak off the collecting capacitor. This leakage is minimized by use of the feedback d.c. amplifier which keeps

the signal lead of the integrator cable near ground potential at all times, and by the automatic recycling which keeps the capacitor from being charged to an excessively high voltage.

Uncertainties in the number of elastically scattered particles arise from scattering out of the scattered beam due to multiple scattering and also from detection of inelastically scattered particles. Some of the elastically scattered particles are absorbed in the scattering target and in the energy attenuator. The absorption in the energy attenuator is accounted for in the measurement of the energy attenuator effect in the direct beam. Absorption in the thin scattering targets is negligible.

Cladis, Hadley, and Moyer[17] have observed "quasi-elastically" scattered protons from several target materials, having energy and angular distributions appropriate to free nucleon-nucleon collisions. If these collisions were with stationary nucleons, their energy would go as $\cos^2 \theta$ and they would not be detected in the proton telescope of this experiment, because of the setting of the energy threshold with energy attenuators. The data of Cladis, et al. indicate a spread in energy attributable to the Fermi energy of the nucleons in the nucleus, which is sufficient that some of the particles which are quasi-elastically scattered may have enough energy to get through the proton telescope. The detection threshold used in this experiment is 330 Mev, so it is believed that not an appreciable number of the quasi-elastic protons get through. Some of the early runs were made with 315 Mev threshold. The results of those runs are not statistically different from those made at the higher threshold.

---

17 J. B. Cladis, J. W. Hadley, and B. J. Moyer, Phys. Rev. 81, 649 (A), (1951)

C. Energy Threshold

It is not possible to determine exactly the detection threshold of the apparatus because of straggling in the energy attenuator. For convenience, the same energy attenuator is used in all runs having the same angular resolution. For the better angular resolution curves which are included in this report, the energy loss in the scatterers, which were chosen so as to have multiple scattering angles appropriate to the angular resolution desired, varied by a few Mev. This means that the detection threshold was not exactly the same for all elements. The variation is so small as to be unimportant. The same energy attenuator was used for all angles. Since the correction for center of mass motion is small, the variation of energy of elastically scattered protons with angle is relatively unimportant. As an extreme example, the energy decrease due to center of mass correction is only about 5 Mev for C at 30°. Nearly all of the datum points included in this paper are at smaller angles than this, where the effect is not even this large.

D. Double Scattering in Target

An uncertainty not yet considered is the possibility of a proton experiencing two wide-angle scattering events in the target, thus appearing at the wrong angle. The probability for a double scattering into an angle θ is proportional to the product of the probability of scattering into an angle α and that for scattering into β, where $\theta = \alpha + \beta$. This should be negligible for thin targets and for the angles considered.

E. Rutherford Scattering into Large Angles

The differential cross section for Rutherford scattering of protons

by a point source of Coulomb field is given classically by[18]

$$\frac{d\sigma}{d\Omega}(\theta) = \left[\frac{Ze^2}{2Mv^2}\right]^2 \frac{1}{\sin^4 \frac{1}{2}\theta} \qquad (14)$$

where Z is the charge of the scattering center in electronic charges, e is the electronic charge, M is the reduced mass of the system, and v is the velocity of approach of the proton. E. J. Williams[19] has considered the relativistic case and has corrected for the finite size of the nucleus, considering the charge to be uniformly distributed throughout the nucleus. The corrected formula which he gives is:

$$\frac{d\sigma}{d\Omega}(\theta) = \left[\frac{Ze^2}{2M\gamma\beta^2c^2}\right]^2 \frac{1}{\sin^4 \frac{1}{2}\theta} \frac{1}{\left[1 + \left(\frac{b}{\lambda\!\!\!^{-}} \sin \frac{1}{2}\theta\right)^2\right]^2} \qquad (15)$$

where β is v/c, γ is $\sqrt{1-\beta^2}$, c is the velocity of light, b is the nuclear radius, and $\lambda\!\!\!^{-}$ is the reduced DeBroglie wavelength of the incident proton. This formula gives cross sections of 6.7×10^{-25} cm^2 and 7.9×10^{-26} cm^2 at 6° and 8° respectively from Pb. These cross sections are down by a factor of about thirty from the values measured in this experiment. For C at 10° the factor is greater than one hundred.

Mr. K. M. Gatha is at present undertaking the solution of the wave equation including both the Coulomb and nuclear effects and considering transparency. His preliminary results indicate that the Coulomb effect should be important only up to about 2° for C and 6° for Pb.[20]

---

[18] Schiff, op. cit., page 117

[19] E. J. Williams, Proc. Roy. Soc. 169A, 531 (1939)

[20] K. M. Gatha, Private communication

It is interesting to set an approximate upper limit upon the angle at which a proton may scatter by Rutherford scattering. The maximum sidewise momentum which the proton may acquire in the collision is proportional to the square root of the Coulomb barrier energy of the struck nucleus. The square root of the ratio of the barrier energy to the total kinetic energy (incident energy) will then give an approximate upper limit to the angle. For 340 Mev protons incident upon Pb, this angle is about 12°, while for C it is about 5°.

The angular distribution of multiply Coulomb scattered particles is Gaussian. The probability for multiple Coulomb scattering into an angle greater than twice the half-width at half maximum of the Gaussian is less than the probability for single Rutherford scattering into the same angle, which has been shown to be negligible.[19]

VIII CONCLUSIONS AND COMPARISON WITH THEORY

A. Angular Distributions

The angular distributions are seen to give diffraction patterns as expected, except for C. It is even possible to detect a minimum for C, but the datum points are not close enough together to make the minimum certain. Since the transparent nucleus theory considers a model in which the nucleus is a sphere with an index of refraction, the model probably does not hold for such a light nucleus with its small number of nucleons. The results of this experiment indicate that C appears quite "open" to the 340 Mev protons.

The relative heights of the secondary maxima of succeeding orders agree favorably with diffraction theory for those elements in which two

secondary maxima have been observed. The minima appear at slightly larger angles than in the theoretical curves, indicating that the nuclei are probably even more transparent than assumed in the transparent nucleus theory.

The 83 Mev neutron results may be matched by a nuclear radius given by $R = 1.39 \times 10^{-13} A^{1/3}$ cm. If the nuclear radii are calculated by Equation (7), using the positions of the first minima found in this experiment, it is found that the radii of opaque nucleu which would give minima at those positions would be given by a coefficient which varies from 0.84 for C to 1.13 for Pb. This is again an indication of nuclear transparency.

B. Total Cross Sections for Elastic Scattering

The total cross sections for nuclear scattering, omitting the Coulomb part, were determined by counting squares on a curve of cross section per unit angle $\left(\frac{d\sigma}{d\theta} = \frac{d\sigma}{d\Omega}(\theta)\, 2\pi \sin\theta\right)$ plotted as a function of angle. Although the total solid angle offered at large angles is much greater than that at small angles, the cross sections fall off rapidly enough that the contribution for angles greater than 30° is negligible in all cases. The results of the integration are consistent with the neutron results. It should be emphasized again that the continuation of the curves and the integration were done systematically, without regard to the expected answer.

C. Nuclear Quadrupole Moment

The high spin nuclei show no statistically important differences from their zero-spin neighbors, excapt that the Al minimum appears slightly sharper. The resolution is such that nuclear eccentricities of less than 10 percent should not be discernible.

IX ACKNOWLEDGMENTS

The author wishes to thank Professor Burton J. Moyer for his kind guidance and assistance throughout this experiment. Mr. Cecil E. Leith, Jr., was very helpful in the planning and initiating of the experiment. Mr. William P. Ball has been of great assistance in helping with the collection of data. Many interesting discussions concerning the nuclear models and the theoretical interpretations have been held with Mr. K. M. Gatha and Mr. S. Fernbach. Finally the author wishes to express his gratitude to the American Taxpayers who have so kindly supported this research through the United States Atomic Energy Commission.